



The pre-Campi Flegrei caldera (>40 ka) explosive volcanic record in the Neapolitan Volcanic Area: New insights from a scientific drilling north of Naples, southern Italy

Domenico Sparice^{a,*}, Carlo Pelullo^a, Sandro de Vita^a, Ilenia Arienzo^a, Paola Petrosino^b, Angela Mormone^a, Gianfranco Di Vincenzo^c, Barbara Marfè^a, Bruna Cariddi^a, Maddalena De Lucia^a, Enrico Vertechì^a, Claudia D'Orlando^d, Paola Del Carlo^d, Alessio Di Roberto^d, Biagio Giaccio^e, Giovanni Zanchetta^f, Mauro Antonio Di Vito^a

^a Istituto Nazionale di Geofisica e Vulcanologia, Sezione di Napoli Osservatorio Vesuviano, via Diocleziano 328, 80124 Naples, Italy

^b Dipartimento di Scienze della Terra, dell'Ambiente e delle Risorse, Università degli Studi di Napoli Federico II, via Vicinale Cupe Cintia 21, 80126 Naples, Italy

^c Istituto di Geoscienze e Georisorse, Consiglio Nazionale delle Ricerche, Via Moruzzi 1, 56124 Pisa, Italy

^d Istituto Nazionale di Geofisica e Vulcanologia, Sezione di Pisa, via C. Battisti 53, 56125 Pisa, Italy

^e Istituto di Geologia Ambientale e Geoingegneria, Consiglio Nazionale delle Ricerche, Montelibretti, Rome, Italy

^f Dipartimento di Scienze della Terra, Università di Pisa, via S. Maria, 56126 Pisa, Italy

ARTICLE INFO

Keywords:

Neapolitan Volcanic Area
Campi Flegrei
Pre-caldera volcanism
Scientific drilling
X-ray powder diffraction
⁴⁰Ar/³⁹Ar dating

ABSTRACT

The oldest volcanism documented in near-vent sections around the Campi Flegrei (CF, southern Italy) caldera does not exceed ~78 ka, even though the mid- to ultra-distal tephrostratigraphic record would suggest that activity in this area started well before that. Reconstructing the activity preceding the large caldera-forming Campanian Ignimbrite (CI) eruption of ~40 ka, via surface geological surveys in proximal areas, is challenging because of the poor accessibility and paucity of sections recording the older chronostratigraphic interval. In order to fill the gap in knowledge of the activity preceding the CI eruption, a 113.2 m deep scientific drillhole was emplaced in the Ponti Rossi area, in the northern part of the city of Naples. The Ponti Rossi area was selected as representative of the stratigraphic setting prior to the CF caldera formation because it is close, although external, to any proposed caldera rim or downthrown area. The cored succession, consisting of pyroclastic deposits separated by paleosols, reworked humified deposits or subaerial erosional surfaces, has been logged and sampled for sedimentological, mineralogical, and geochronological analyses. Thirty-one Pyroclastic Units (PU) were identified. Based on the structural/textural features of the recovered sediments, the first relevant result is the possible absence of the CI, while the deposits of the ~15 ka Neapolitan Yellow Tuff eruption, the second largest caldera-forming event of CF, represent the shallowest sediments. ⁴⁰Ar/³⁹Ar age determinations on alkali feldspars, extracted from juvenile fragments collected at 45.8–45.9 (PU-29) and 99.5–99.6 (PU-1) metres of depth, yielded ages of 59.03±0.50 ka and 110.00±0.35 ka, respectively. The age obtained for the deepest cored unit, having sedimentological characteristics compatible with proximal deposition, represents the oldest age obtained for a pyroclastic deposit in the sequences near the CF caldera boundaries and extends by 30 ky the explosive history of this area. Furthermore, based on ⁴⁰Ar/³⁹Ar age constraints, at least 29 eruptions, spanning the ~59–110 ka interval, can be added to the volcanic history of the Neapolitan Volcanic Area. These eruptions can be largely attributed to the CF area, prior to the CI caldera formation, and testify to hitherto unknown, intense explosive activity.

1. Introduction

Reconstructing the eruptive history of an active volcanic area,

through detailed stratigraphical and geochronological investigations, is pivotal for accurate knowledge of type, size, and frequency of eruptions, which in turn represent crucial data for volcanic hazard assessment in

* Corresponding author.

E-mail address: domenico.sparice@ingv.it (D. Sparice).

<https://doi.org/10.1016/j.jvolgeores.2024.108209>

Received 20 July 2024; Received in revised form 11 October 2024; Accepted 12 October 2024

Available online 18 October 2024

0377-0273/© 2024 The Author(s). Published by Elsevier B.V. This is an open access article under the CC BY license (<http://creativecommons.org/licenses/by/4.0/>).

densely populated regions (e.g., Cioni et al., 2003; Orsi et al., 2004, 2009; Lirer et al., 2010; Alberico et al., 2011; Bevilacqua et al., 2022a). Nevertheless, exploring the older volcanic activity is a challenging task because field-based studies often provide only a partial reconstruction, limited to the most recent and/or voluminous volcanism. Deposits of past eruptions may occur in a few scattered outcrops preserved in non-volcanic successions in medial-distal settings (e.g., Di Vito et al., 2008; Zernack et al., 2011; Németh and Palmer, 2019; Monaco et al., 2022a) or may be buried/eroded by the emplacement of younger pyroclastic deposits in near-vent areas. In addition, large explosive eruptions may result in a volcano-tectonic collapse, which further degrades the proximal stratigraphic record, usually partially preserved along the caldera margins (e.g., Orsi et al., 1996; Perrotta et al., 2006, 2010; Branney and Accocella, 2015; Gooday et al., 2018; Vineberg et al., 2023). This may result in under-estimation of eruptions, which worsens back in time, and can pose relevant issues in properly assessing the long-term volcanic hazard and determining return periods over a very long-time scale.

The situation is even more complex in caldera systems that may result from multiple (nested) collapses (e.g., Geyer and Martí, 2009;

Cole et al., 2005) such as the Campi Flegrei (CF) caldera (e.g., Orsi et al., 1996; Vitale and Isaia, 2014), which, moreover, is located very close to the other peri-contemporaneous active volcanoes of Ischia, Procida and Vesuvius. The CF caldera (Fig. 1) is conventionally interpreted as the result of two nested caldera collapses (Orsi et al., 1996) related to the Campanian Ignimbrite (CI; 39.28 ± 0.11 ka, De Vivo et al., 2001, recalculated at 39.85 ± 0.11 ka; 39.85 ± 0.14 ka, Giaccio et al., 2017a) and the Neapolitan Yellow Tuff eruption (NYT; 14.9 ± 0.4 ka, Deino et al., 2004; $14.38\text{--}13.98$ ka, Matthews et al., 2015). The last ~15 ka of volcanic activity at CF has been thoroughly investigated (e.g., Di Vito et al., 1999; Smith et al., 2011; D'Antonio et al., 2022 and references therein) whereas, due to the lack of extensive exposures, only fragmentary information exists regarding the stratigraphic record preceding the caldera formation. The CI eruption is the largest eruptive event sourced from the Neapolitan area, with VEI 7 and estimated Magnitude (M) between 7.2 and 7.7 (Marianelli et al., 2006; Scarpati et al., 2014; Silleni et al., 2020). Its deposits in the Campanian region consist of a decametre-thick, welded to lithified, grey to yellow ignimbrite sheet (e.g., Di Girolamo, 1970; Barberi et al., 1978; Fisher et al., 1993; Fedele

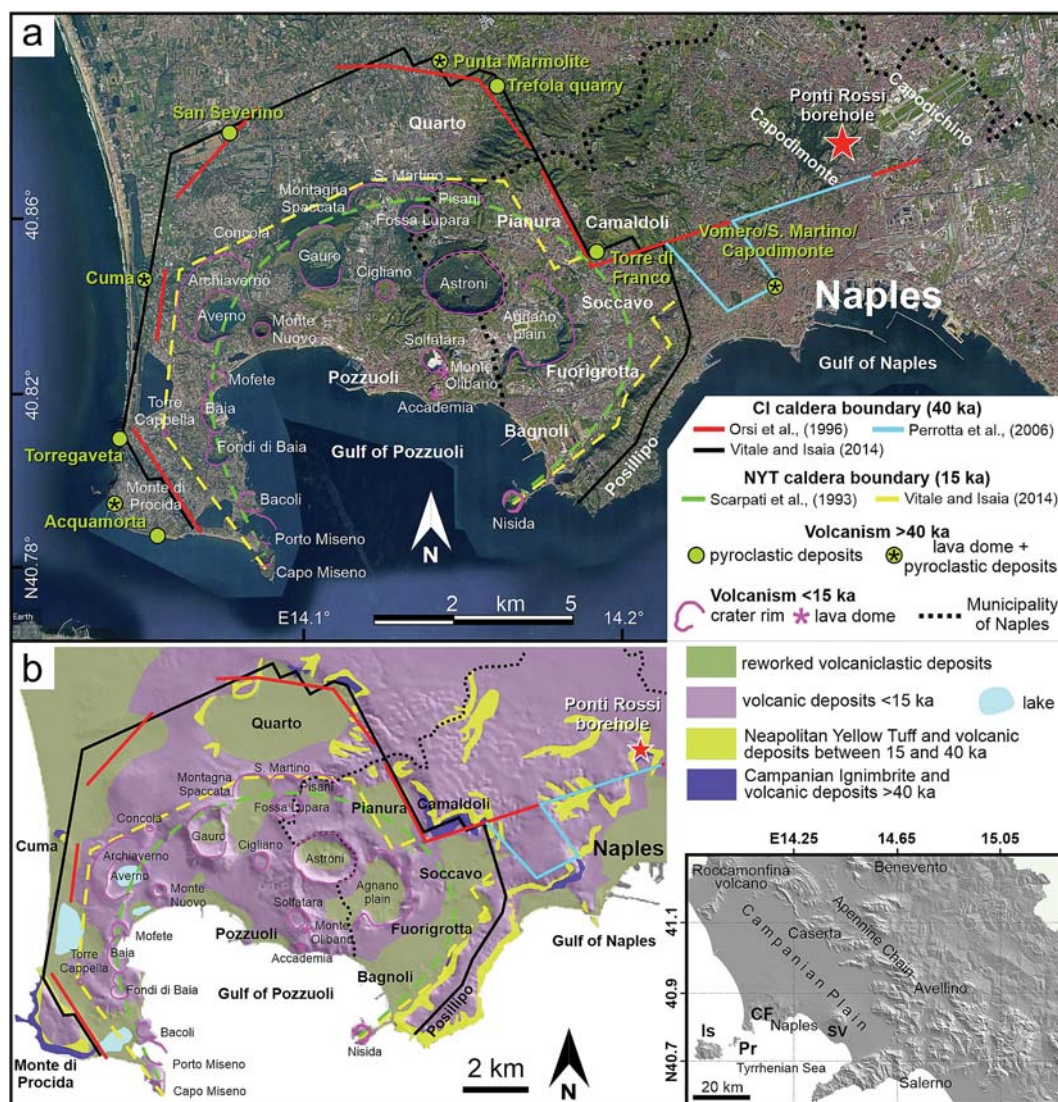


Fig. 1. a) Map (Google Earth) and b) simplified geological map of Campi Flegrei (after Orsi et al., 1996 and Isaia et al., 2019) and location of the Ponti Rossi borehole (red star) in the northern part of the municipality of Naples. The Campanian Ignimbrite (CI) and Neapolitan Yellow Tuff (NYT) caldera boundaries, according to different authors, are reported as well as proximal sites where volcanic deposits >40 ka crop out. Inset: Location of the Neapolitan volcanoes (in bold) in the Campania region (southern Italy); CF = Campi Flegrei, Is = Ischia Island, Pr = Procida Island, SV = Somma-Vesuvius. (For interpretation of the references to colour in this figure legend, the reader is referred to the web version of this article.)

et al., 2016; Rolandi et al., 2020; Scarpata et al., 2020; Silleni et al., 2020, 2024) overlying a Plinian fall deposit dispersed toward the east (Rosi et al., 1999; Scarpata and Perrotta, 2016; Scarpata et al., 2016). Proximal deposits, cropping out along the CI caldera rim (Fig. 1), consist of a thick sequence of eutaxitic ignimbrite (Piperno facies *Auct.*; Maggione, 1934; Rittmann, 1950), coarse lithic breccias and matrix-supported, unconsolidated pumice-flow deposits (e.g., Perrotta and Scarpata, 1994; Melluso et al., 1995; Fedele et al., 2008).

In this context, scientific drillholes represent the most valuable tool to investigate the deep stratigraphic record resulting from past eruptions (e.g., Brocchini et al., 2001; Di Renzo et al., 2007; De Natale et al., 2016; Sacchi et al., 2019) in proximal-intermediate areas. In order to fill the gap in knowledge of the volcanic activity preceding the CI caldera collapse, a scientific drillhole was emplaced in the Ponti Rossi area (Fig. 1), in the northern part of the city of Naples, in the framework of the INGV – Pianeta Dinamico TIFEHO (Trachytic Ignimbrites magma-chambers Formation and Evolution in the pre-Holocene history of the Campania volcanic area) project, whose main goal is to investigate the volcanic activity older than high magnitude, caldera-forming eruptions in the Neapolitan Volcanic Area. The latter is hereafter referred to as the area that gave rise to the volcanism that preceded the CI eruption according to the nomenclature reported by Pelullo et al. (2024). In this work, we present the detailed stratigraphy of the Ponti Rossi borehole, along with the structural/textural features and mineralogical characterization of the cored units, and $^{40}\text{Ar}/^{39}\text{Ar}$ age determinations on two samples collected from selected units (which include the deepest one). The drilled succession provided evidence for a significant volcanic activity preceding the CI eruption that extends at least 30 ky further back in time than the oldest previously known explosive activity in the CF area.

2. Geological setting and volcanic activity of Campi Flegrei

2.1. Structural setting

CF represents the continental portion of a late Pleistocene to Holocene volcanic district that also comprises the islands of Ischia and Procida, off the Gulf of Naples (e.g., Orsi et al., 1996; Sbrana et al., 2021) (Fig. 1). The CF area is located along the Tyrrhenian Sea margin of the Campanian Plain (Fig. 1), a 35-km-wide Pliocene-Pleistocene structural depression bounded by Mesozoic carbonate ridges (e.g., Scandone et al., 1991; Santangelo et al., 2017), which has been the site of intense volcanism following a stage of extensional tectonics connected to the Tyrrhenian Sea opening (e.g., Vitale and Isaia, 2014; Vitale and Ciarcia, 2018; Milia and Torrente, 2020).

The exact onset of the volcanism in the Campanian Plain is not well constrained although ignimbrite-forming activity dates to at least 290 ka (e.g., De Vivo et al., 2001; Rolandi et al., 2003; Belkin et al., 2016). The conventional view (e.g., Barberi et al., 1991; Orsi et al., 1996; Sbrana et al., 2021; Orsi, 2022) suggests that the present-day morpho-structure of CF is dominated by a 12-km-wide volcano-tectonic depression (caldera), formed as a consequence of the CI and NYT eruptions, the limits of which extend both on land and offshore (e.g., Orsi et al., 1996; Vitale and Isaia, 2014; Steinmann et al., 2016; Natale et al., 2022a, 2022b). The inferred collapsed area during the CI eruption is still not well constrained, particularly regarding its eastern boundary in the city of Naples (Fig. 1). Some authors include the western and central part of Naples in the collapsed area (Orsi et al., 1996; Perrotta et al., 2006) while other authors suggest a roughly semi-circular caldera boundary not incorporating the central sector of the city (Rosi and Sbrana, 1987; Vitale and Isaia, 2014; De Natale et al., 2016; Sbrana et al., 2021). The different models concerning the structural setting of the CI caldera were crucial for the selection of the drilling site as the drillhole was emplaced outside any caldera rim and/or downthrown area.

2.2. Post-CI and post-NYT activity

In the time span between the CI and NYT eruptions, at least 9 explosive events occurred. This explosive activity mainly resulted in a pyroclastic succession referred to as “Tufi Biancastri” (Whitish Tuffs; Rittmann, 1950). This succession consists of pyroclastic units, alternating pyroclastic current and fall deposits, separated by paleosols representing periods of quiescence. One of the eruption units (the fourth unit above the CI in the Ponti Rossi area) belonging to the “Tufi Biancastri” succession has been correlated to a widespread ash layer (Y-3 tephra), showing a Phlegraean geochemical signature. The dispersal of this ash layer in the Mediterranean area and the calculated volume ($\sim 17 \text{ km}^3$ DRE) suggested the occurrence of a third caldera-forming eruption at $29.3 \pm 0.7 \text{ ka}$ ($\pm 2\sigma$), associated with a deposit named Masseria del Monte Tuff, although no proximal evidence of a caldera collapse exists (Albert et al., 2019). On the other hand, the Y-3 ash layer was dated at $\sim 30\text{--}31 \text{ ka}$ by Zanchetta et al. (2008) and correlated to the first unit above the CI (unit VRa) in the Verdolino quarry (Orsi et al., 1996). Following the NYT eruption, eruptive activity was mainly characterized by medium- to small-scale, magmatic to phreatomagmatic and minor effusive eruptions grouped into three main epochs (Di Vito et al., 1999; Smith et al., 2011) separated by long periods of quiescence. The vents of this $<15 \text{ ka}$ activity, comprising at least 70 eruptions, were mainly clustered within the NYT caldera and along its boundaries (Fig. 1) (e.g., Orsi et al., 1996; Di Vito et al., 1999). The largest post-NYT eruptive events are the $\sim 12 \text{ ka}$ Pomici Principali eruption and the $\sim 4.5 \text{ ka}$ Agnano Monte Spina eruption (Di Vito et al., 1999; Orsi et al., 2009). The latter was also responsible for a small volcano-tectonic collapse forming the Agnano Plain (Fig. 1) in the eastern sector of the CF caldera (de Vita et al., 1999). The last CF eruption occurred in 1538 CE and produced the Monte Nuovo tuff cone (e.g., Di Vito et al., 1987, 2016; D’Orlando et al., 2005; Piochi et al., 2005). Volcanic activity within NYT caldera has been coupled with significant long-term ground deformation, mainly in its central part, that alternated between uplift and subsidence, started soon after the NYT eruption and is still ongoing (e.g., Di Vito et al., 1999; Isaia et al., 2019; Tramelli et al., 2022; De Martino et al., 2021; Bevilacqua et al., 2022b). Following the 1970–72 and 1982–84 bradyseismic unrests (e.g., Scarpa et al., 2022), since 2005 a new inflation phase started at CF (e.g., Astor et al., 2024), whose current activity is characterized by shallow seismicity, degassing and geothermal activity (e.g., Piochi et al., 2014; Chiodini et al., 2021; Isaia et al., 2021; Tramelli et al., 2022; Bevilacqua et al., 2022b; Giacomuzzi et al., 2024; Del Pezzo and Bianco, 2024).

3. Volcanism prior to the CI: an overview

Volcanism predating the CI eruption in the Neapolitan Volcanic Area is related to the activity of CF, Ischia and Procida (Fig. 2). These volcanic sources produced caldera-forming eruptions, monogenetic volcanoes, lava domes, and widely dispersed, sheet-like pyroclastic deposits (e.g., Sbrana et al., 2018, 2021; De Astis et al., 2004). The Somma-Vesuvius volcano can be excluded as a possible source, being younger than 40 ka. The stratigraphic record from boreholes (e.g., Brocchini et al., 2001; Di Renzo et al., 2007) highlights that the growth of Somma-Vesuvius postdates the CI eruption, although pyroclastic deposits and lavas older than 40 ka (the oldest lavas have been dated between 300 and 400 ka) have been intersected, representing evidence of ancestral volcanism occurred in the area currently occupied by Somma-Vesuvius.

The prevailing wind pattern in the Neapolitan region is toward the NE-SE quadrant and the same dispersal direction characterizes the distribution of the pyroclastic products vented from the Neapolitan volcanoes, both younger (e.g., de Vita et al., 1999; Isaia et al., 2004; Orsi et al., 2004) and older (Di Vito et al., 2008) than CI (including the CI fall deposit, Rosi et al., 1999; Scarpata and Perrotta, 2016). For this reason, the medial/distal exposures of pre-CI pyroclastic units are mostly confined in a NE-SE sector from the source area (e.g., Di Vito et al., 2008;

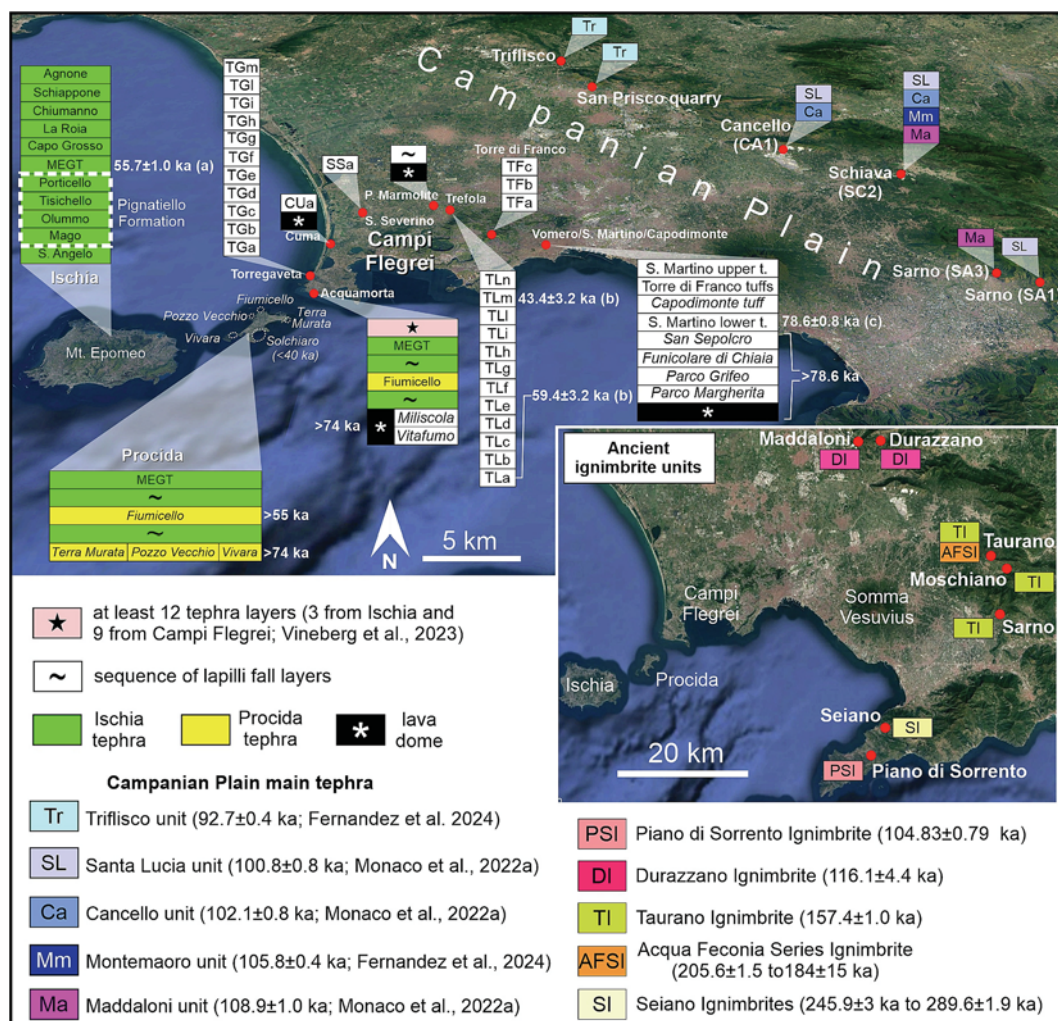


Fig. 2. Map showing the location of the proximal to mid-distal pyroclastic sequences older than the ~40 ka Campanian Ignimbrite in both the continental and insular sector of the Campi Flegrei district. Monogenetic edifices (tuff cones and tuff rings) are reported in italics. Source of stratigraphic data: Cuma, San Severino, Punta Marmolite, Trefola, Torre di Franco (Orsi et al., 1996); Torregaveta (Pappalardo et al., 1999); Acquamorta (Perrotta et al., 2010; Vineberg et al., 2023); Vomero/San Martino/Capodimonte (Perrotta et al., 2006; Scarpati et al., 2013, 2015); Procida (De Astis et al., 2004; Perrotta et al., 2010); Ischia (Brown et al., 2008); Campanian Plain main tephra (Di Vito et al., 2008; Monaco et al., 2022a; Fernandez et al., 2024). Age data (⁴⁰Ar/³⁹Ar) of proximal tephra: (a) Giaccio et al. (2017b); (b) Pappalardo et al. (2002); (c) Scarpati et al. (2013). Ages are recalculated relative to an ACs age of 1.1848 Ma (Niespolo et al., 2017) adopted in this study. The age of the monogenetic volcanoes is based on field stratigraphic relationships: Procida and Acquamorta (Perrotta et al., 2010); Vomero/San Martino/Capodimonte (Scarpati et al., 2013, 2015). Inset: Location and age of ancient ignimbrite units (De Vivo et al., 2001; Rolandi et al., 2003; Belkin et al., 2016). (For interpretation of the references to colour in this figure legend, the reader is referred to the web version of this article.)

Monaco et al., 2022a; Fernandez et al., 2024).

An overview of the pre-CI volcanism at Campi Flegrei, Ischia and Procida is provided below, while schematic logs of the stratigraphic successions >40 ka are illustrated in Fig. 2.

3.1. Campi Flegrei

Results of field surveys highlighted that pre-CI volcanism in the CF area produced mainly explosive eruptions and minor effusive eruptions forming lava domes (e.g., Orsi et al., 1996 and references therein). Exposures of volcanic deposits older than 40 ka occur in scattered sites from proximal (CF caldera rim associated to CI eruption) to medial/distal settings (Apennine Chain) although their stratigraphic correlation is poorly investigated and unclear. Sub-surface geology, investigated through borehole data both inside and outside the caldera, shows evidence of pre-CI volcanism as well (e.g., Orsi et al., 1996; Pappalardo et al., 2002; Bellucci et al., 2006; Perrotta et al., 2006; De Natale et al., 2016). In proximal sites, pre-CI volcanic deposits crop out in a few natural exposures and quarries along the scarps bordering the CI

caldera, moving clockwise from west to east (Fig. 1): Monte di Procida (Acquamorta and Torregaveta), Cuma, San Severino, Punta Marmolite, Trefola quarry, Torre di Franco, Vomero/San Martino/Capodimonte hill (e.g. Rosi et al., 1983; Lirer et al., 1987; Orsi et al., 1996; Pappalardo et al., 1999; Perrotta et al., 2006, 2010; Scarpati et al., 2013, 2015). The oldest dated tephra (San Martino Lower Tephra), tentatively attributed to Plinian activity, collected from a pyroclastic sequence at the base of the San Martino hill (Fig. 2) in the city of Naples, yielded an age of 78.66 ±0.88 ka (Scarpati et al., 2013). In the nearby areas, older undated deposits are represented by at least four monogenetic cones (Parco Margherita, Parco Grifeo, Funicolare di Chiaia and San Sepolcro; Fig. 2), plus a buried lava dome, forming the hilly morphology of the city of Naples (Romano et al., 2013; Scarpati et al., 2013, 2015). Similarly, along the Monte di Procida promontory (Fig. 2), to the south-west of the CI caldera rim, two tuff cones (Vitafumo and Miliscola, Perrotta et al., 2010; Santangelo et al., 2024) and a lava dome represent the oldest (>74 ka) volcanic landforms in the stratigraphic record, mantled by a thick sequence of pyroclastic fall layers and tuff deposits, attributed to the activity of Ischia, Procida and CF, in turn capped by the proximal CI

deposits (e.g. Rosi and Sbrana, 1987; Orsi et al., 1996; Pappalardo et al., 1999; Perrotta et al., 2010; Vineberg et al., 2023). A thick succession formed by twelve superimposed pre-CI pyroclastic units, named Trefola-a to Trefola-n (TLa to TLn), separated by humified horizons, well-developed paleosols and reworked material, is reported at Trefola quarry (Fig. 2) dug at the base of a scarp representing the northern sector of the CI caldera rim (Orsi et al., 1996; Pappalardo et al., 1999; Pabst et al., 2008). Single units vary in thickness from a few centimetres to 15.3 m. Some units (TLb, TLc, Tlf and Tlm; Fig. 2), composed of both fall and pyroclastic current deposits, show characteristics compatible with proximal deposition as impact sags or features related to sedimentation from high-energy pyroclastic currents, while other units (Tld, Tle, Tlg, Tlh and Tli; Fig. 2) are referred to as distal fall deposits (Orsi et al., 1996). $^{40}\text{Ar}/^{39}\text{Ar}$ geochronological determinations on the lowermost unit (TLa), described as a pyroclastic flow deposit, yielded an age of 58 ± 3 ka, while the deposits immediately underlying the CI were dated at 45.6 ± 0.7 (Pappalardo et al., 1999). In medial/distal settings, exposures of pre-CI deposits are reported from 30 km as far as 55 km from CF, along the first offshoots of the reliefs bordering the Campanian Plain and beyond the Apennine Chain (Romano et al., 1994; Bellucci et al., 2003; Di Vito et al., 2008; Monaco et al., 2022a). Most of medial/distal pre-CI units tentatively attributed to CF activity, consisting of stratified fall deposits of coarse ash to pumice lapilli with scarce lithic fragments, are described by Di Vito et al. (2008). Five of these pyroclastic units (Triflisco, Santa Lucia, Canello, Montemaoro and Maddaloni; Fig. 2) have been recently geochemically and geochronologically fully characterized and correlated to some well-known Mediterranean tephra markers, preserved in the Marine Isotope Stage 5 (MIS 5) tephrostratigraphic record, and dated between ~ 92 and ~ 109 ka (Monaco et al., 2022a; Fernandez et al., 2024). Different ignimbrite units (Fig. 2), locally associated with fall deposits, dated between ~ 105 and ~ 290 ka, were mainly recognised at the foothills of the Apennine Chain (De Vivo et al., 2001; Rolandi et al., 2003; Belkin et al., 2016) as well as in boreholes and through seismic profiles (e.g., Aprile and Toccaceli, 2002; Aprile et al., 2004; Torrente et al., 2010; Pennetta et al., 2014). The age, and related uncertainties, of such ignimbrite units are listed as reported by De Vivo et al. (2001), Rolandi et al. (2003) and Belkin et al. (2016). The oldest of these ignimbrite units (Fig. 2) are the three flow units named Seiano Ignimbrites (245.9 ± 3 ka to 289.6 ± 1.9 ka). The lowest unit rests directly on the Mesozoic carbonate basement of the Sorrento peninsula and is separated from the upper units by a paleosol. The other ignimbrite units are the 157.4 ± 1.0 ka Taurano Ignimbrite, the 116.1 ± 4.4 ka Durazzano Ignimbrite and the 104.83 ± 0.79 ka Piano di Sorrento Ignimbrite. In one locality (Fig. 2), the Taurano Ignimbrite is underlain by a sequence composed of incoherent ash beds in turn resting on layered tuffs. The sequence below the Taurano Ignimbrite is grouped in the “Acqua Feconia Series Ignimbrite” (Fig. 2; Belkin et al., 2016) and dated between 205.6 ± 1.5 and 184 ± 15 ka (De Vivo et al., 2001). While these ancient ignimbrites are thought to have been vented from the Campanian Volcanic Zone (Rolandi et al., 2003), which roughly corresponds to the Campanian Plain, in other recent studies they are tentatively attributed to the CF or the Neapolitan Volcanic Area activity (Monaco et al., 2022a; Fernandez et al., 2024). Such explosive volcanism has also been recognised as distal and ultra-distal tephra and crypto-tephra in both marine and terrestrial tephrostratigraphic records (e.g. Wulf et al., 2006, 2012; Giaccio et al., 2012, 2017b; Insinga et al., 2014; Di Roberto et al., 2018; Petrosino et al., 2016, 2019; Monaco et al., 2022b; Fernandez et al., 2024), further testifying to the occurrence of a significant past explosive activity, whose near-vent/medial record is fragmentary and source eruptions are still mostly unknown.

3.2. Ischia Island

Volcanism at Ischia Island covers a period of more than 150 ky (e.g. de Vita et al., 2010; Sbrana et al., 2018) with the last eruption occurred in 1302 CE (Arso eruption). Several pyroclastic units sourced from Ischia

extensively blanket also the nearby Procida Island and Monte di Procida (Fig. 2) promontory (e.g., Rosi et al., 1988; Brown et al., 2008; Perrotta et al., 2010). In the period 150–74 ka, volcanic activity occurred through effusive eruptions, which produced lava flows and lava domes, and explosive (Plinian) eruptions that produced several pyroclastic units separated by paleosols (e.g., de Vita et al., 2010; Sbrana et al., 2018). Paroxysmal explosive volcanism occurred in the 74–55 ka interval, forming a succession of thick Plinian pumice fall deposits separated by paleosols, known as Pignatiello Formation (Fig. 2), shortly followed by the ~ 56 –54 ka Monte Epomeo Green Tuff (MEGT, Fig. 2) caldera-forming eruption, the largest eruptive event sourced from Ischia (e.g., Brown et al., 2008, 2014; Tomlinson et al., 2014; Sbrana et al., 2018). The composite MEGT extracaldera sequence consists of a basal Plinian pumice fall deposit overlain by an ignimbrite and a lithic breccia (Brown et al., 2008). MEGT is also one of the main tephra markers in the Mediterranean tephrostratigraphic record (e.g., Tomlinson et al., 2014, 2015; D’Antonio et al., 2021). After MEGT, high-energy explosive (Plinian) and minor explosive to effusive activity occurred, separated by periods of quiescence (Brown et al., 2008; Sbrana et al., 2018; Fig. 2). About 46 eruptions occurred during the last 10 ka, generating lava flows and domes, scoria cones, tuff rings and tuff cones and widespread sheets of ash and pumice lapilli (de Vita et al., 2010). Medial/distal occurrences of at least two Ischia tephra (SMP1-a and SC2-a; Di Vito et al., 2008) are reported on the Apennines. One of them (SC2-a) has been tentatively correlated to a pyroclastic unit of the Pignatiello Formation (Di Vito et al., 2008).

3.3. Procida Island

Procida Island resulted from the activity of four tuff rings (Vivara, Pozzo Vecchio, Fiumicello and Solchiaro) and a tuff cone (Terra Murata), in the time span between >74 and ~ 24 ka, along with the accumulation of exotic pyroclastic products (e.g., Rosi et al., 1988; De Astis et al., 2004; Perrotta et al., 2010; Fig. 2) vented from Ischia and the Ischia Channel (the strait between Ischia and Procida). All these volcanic edifices, except Solchiaro, predate the CI eruption. Vivara, Pozzo Vecchio and Terra Murata are the oldest volcanic centres, dated at >74 ka, being mantled by the fallout sequence attributed to the Pignatiello Formation (originated from Ischia). Deposits of such vents are well exposed only at Procida (Fig. 2). Fiumicello tuff ring (Fig. 2) is sandwiched between two pumice fall deposits belonging to the upper part of the Pignatiello Formation (Fedele et al., 2006). Away from the vent, Fiumicello products are easily traced up to Monte di Procida (Fig. 2) where they are represented by well-stratified scoria lapilli and ash fall deposits (Fedele et al., 2006; Perrotta et al., 2010). Based on the geochemical signature, no occurrence of products sourced from Procida has been recognised in the Campanian Plain and on the Apennine Chain (Di Vito et al., 2008; Monaco et al., 2022b) although a tephra layer, found in the Lago Grande di Monticchio, >100 km East of Procida, has been attributed to the Fiumicello eruption by Wulf et al. (2006). Solchiaro tuff ring, dated at ~ 24 ka (Morabito et al., 2014), represents the last autochthonous activity at Procida.

4. Drilling site selection

The scientific drilling was performed in the Ponti Rossi area (Fig. 1), to the north of Naples, in order to investigate the volcanic stratigraphy preceding the CF caldera formation (>40 ka). The selection of the drilling site (40.875892° Lat; 14.263611° Long; 50 m a.s.l.) was aimed at retrieving a stratigraphic record spanning back in time beyond the oldest rocks cropping out along the CF caldera boundary, dated between ~ 60 and ~ 80 ka (Pappalardo et al., 1999; Scarpati et al., 2013, 2015) and, possibly, at recovering the proximal equivalents of the mid-distal and distal MIS 5 tephra (~ 109 –93 ka) that are reliably attributed to the CF activity (Giaccio et al., 2017b; Monaco et al., 2022a; Fernandez et al., 2024).

The Ponti Rossi area is comprised between Capodichino hill to the east and Capodimonte hill to the west (Fig. 1) and is located to the north of the inferred CF caldera topographic/structural rim of Orsi et al. (1996), just outside the supposed downthrown area in the city of Naples. The rim is represented by a scarp formed due to the partial reactivation of a regional fault system during the CI eruption (Orsi et al., 1996). On the other hand, the selected site is well outside, about 5 km east, of the CF caldera boundary proposed by Rosi and Sbrana (1987), Vitale and Isaia (2014) and De Natale et al. (2016). In light of the different views about the extent of the caldera, the drilling location was chosen because it is external to any hypothesised caldera rim, topographic or structural scarp and downthrown area (Fig. 1). From a stratigraphic point of view, the surface geological record of the Ponti Rossi area, exposed in a currently inhabited area once occupied by a large quarry, comprises a pyroclastic succession from the CI deposits, whose base is not exposed, to deposits younger than NYT (Orsi et al., 1996). In the same area, a pyroclastic succession older than CI was investigated through a ~100-m-deep borehole (S51 borehole) in which eleven pyroclastic units (PRA to PRm), separated by well-developed paleosols, were recognised and described by Pappalardo et al. (1999, 2002), who also provided a geochemical and geochronological characterization. $^{40}\text{Ar}/^{39}\text{Ar}$ age determinations on units underlying the CI in this borehole yielded an age of 44.3 ± 0.7 ka ($\pm 1\sigma$). This age is indistinguishable, within the uncertainties, from the age (45.6 ± 0.7 ka; $\pm 1\sigma$) of the unit directly underlying the CI at Trefola quarry (Pappalardo et al., 1999). In addition, pre-CI deposits were intercepted in other boreholes drilled in the nearby areas (Orsi et al., 1996; Bellucci et al., 2006; Perrotta et al., 2006). According to Orsi et al. (1996), the top of the pre-CI sequence varies in elevation between 15 m b.s.l. and 50 m a.s.l. A similar range of altitude is provided by Bellucci et al. (2006). Conversely, drillings in the inferred collapsed area, immediately to the south of the caldera rim and well inside the city of Naples, did not even penetrate the top of the CI at a depth of hundreds of meters (e.g., Orsi et al., 1996; Alberico et al., 2005; Petrosino et al., 2021). Finally, this area lies well inside the easterly dispersal of the pyroclastic products sourced from both the continental and insular parts of the CF volcanic district. Despite the different views

about the CF caldera and its actual boundaries, all authors agree about the occurrence of thick pre-CI deposits at shallow depth in the area encompassing the Ponti Rossi site, making it the most suitable for a detailed investigation of the stratigraphic record preceding the CF caldera formation in the Neapolitan Volcanic Area.

5. Materials and methods

5.1. Drilling procedure

The drilling procedure was carried out through technical and logistical mud services (Fig. 3a). The drilling reached a maximum depth of 113.2 m below the ground level located at 50 m a.s.l. The borehole was drilled using a continuous coring technique to retrieve a complete core record over the whole borehole length. Core sections were 3 m-long and 10 cm in diameter throughout the drill hole. Casing tubes were necessary starting from 39 m of depth downwards, due to the occurrence of groundwater, in order to ensure the stability of the well. An overall recovery percentage of 98 % provides a detailed stratigraphic record, preliminarily described in the field. In order to preserve their integrity, cores were placed into 1-m-long and 10-cm-diameter PVC half pipes (Fig. 3b), photographed (Fig. 3c), wrapped in a plastic film and then accommodated in plastic boxes. Cores were stored, logged and sampled at the Istituto Nazionale di Geofisica e Vulcanologia-Osservatorio Vesuviano (INGV-OV).

5.2. Stratigraphic criteria and sampling

Stratigraphy in volcanic areas is defined by a superimposition of deposits, resulting from a series of eruptions, usually separated by paleosols, reworked volcanoclastic or non-volcanic deposits, and unconformities, reflecting periods of volcanic quiescence and/or volcanotectonic processes (e.g., Perrotta et al., 2010; Lucchi et al., 2010; Lucchi, 2013; Martí et al., 2018). By combining volcanic and stratigraphic criteria for mapping in volcanic areas, Fisher and Schmincke (1984) proposed “volcanic activity units” having different hierarchies, from a

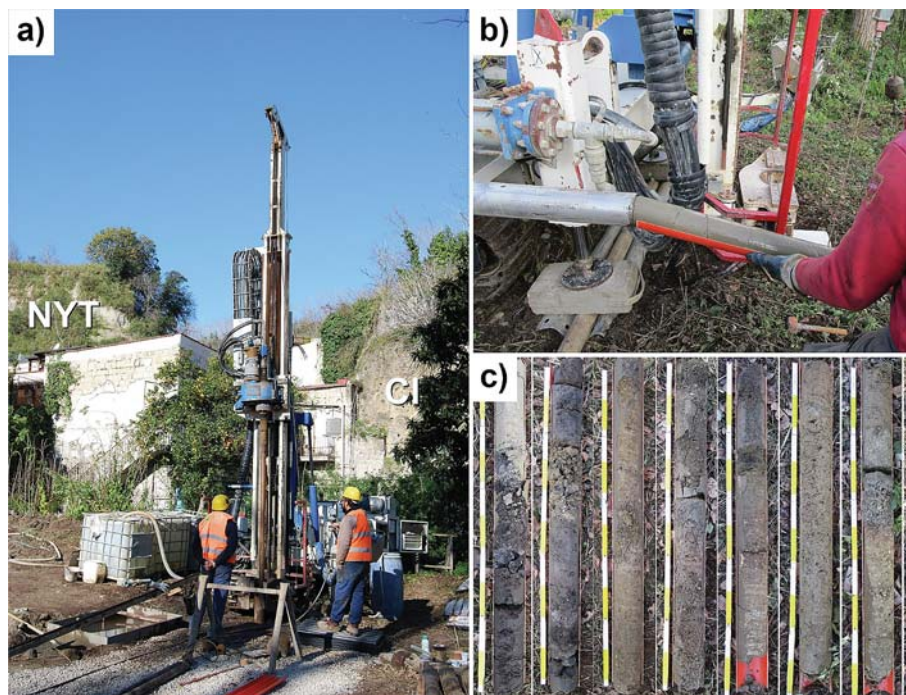


Fig. 3. a) Drilling operations in the Ponti Rossi area (February 2022). In the background, the pyroclastic deposits of the Campanian Ignimbrite (CI) and Neapolitan Yellow Tuff (NYT); b) and c) cored sediments preserved in PVC half pipes. (For interpretation of the references to colour in this figure legend, the reader is referred to the web version of this article.)

single phase of an eruption to an eruptive period including multiple eruptions. For example, volcanic deposits emplaced during a single eruption are usually referred to as “Eruption Unit”. Notwithstanding, very closely spaced eruptions from a single, or multiple sources, would not result in well-developed paleosols or any clearly recognizable physical surface that would indicate a brief break in the volcanic activity. In addition, the occurrence of simultaneous eruptions from different vents several kilometers apart within caldera systems, although infrequent, has been suggested in the recent history of CF (Pistolesi et al., 2016). This would result in an alternation of different tephra layers whose sources cannot be clearly distinguished through a stratigraphic approach, making further analytical investigations necessary, such as geochronological, geochemical and isotopic characterization of the juvenile material, to discriminate the contribution of different discrete eruptions from different vents. For these reasons, we avoid the term “Eruptive Unit” when describing the cored succession, as it may promote a misleading interpretation of the borehole stratigraphy in terms of number of eruptions. We also avoid the term “Lithostratigraphic Unit”, as it is the basic unit for geological mapping and cartography and refers to a mappable body of rocks having diagnostic lithologic features (International Commission on Stratigraphy). Based on these assumptions, the pyroclastic succession drilled at Ponti Rossi has been described following a simple stratigraphic criterion of superposition of deposits that does not imply the interpretation of the stratigraphy in terms of number of eruptions or areal distribution. We generically refer to a “Pyroclastic Unit” (PU) to indicate a pyroclastic deposit or a sequence of deposits, regardless of the emplacement mechanisms (fallout or pyroclastic current), thickness or structure, sandwiched between paleosols/humified reworked deposits or separated by sub-aerial erosional surfaces clearly indicating periods of volcanic quiescence. In this light, a PU can include deposits that, although not separated by any type of physical discontinuity, could result from multiple eruptions, close both in time and space, from different vents/sources; in other words, in our stratigraphy, a PU does not necessarily result from a single eruption. The presence of reworked volcanoclastic deposits, without any evidence of humification/pedogenesis, is not necessarily considered indicative of volcanic quiescence as it could also represent *syn*-eruptive reworking events. The contribution of discrete eruptions, as well as of different sources, will be discriminated through an ongoing detailed geochemical characterization. Each PU has been described based on its internal structure and textural characteristics as well as the lithology of juvenile and lithic fragments. Seventy-seven samples have been collected throughout the sequence to characterize the deposits from a sedimentological (type of juvenile and lithic fragments; Table 1) and mineralogical point of view (Table 2). Samples were labelled with an alphanumeric code formed by the acronym of the drilling site (PR) followed by the sampling-depth interval. Samples from two PUs have been selected for $^{40}\text{Ar}/^{39}\text{Ar}$ age determination.

5.3. Sedimentological analyses

In the Sample Preparation Laboratory of the INGV-OV, samples were oven-dried and mechanically sieved down to 4ϕ (0.063 mm), at 1ϕ intervals ($\phi = \log_2 d$, where d is the diameter of particles in mm). Lithological components were separated by hand-picking down to -1ϕ (2 mm), while the finer fraction was analysed by observation under a binocular microscope. Clasts were separated into three main categories: juveniles, lithics, and loose crystals. Crystals for geochronological analysis were extracted from juvenile fragments and separated from the size classes 1ϕ (0.5 mm) and 2ϕ (0.25 mm).

5.4. X-Ray Diffraction analyses

Following the sedimentological analyses, in order to obtain the mineralogical compositions of the 0ϕ (1 mm) bulk fractions (including loose crystals and lithic fragments) of selected samples, and to compare

them with those of the juvenile material on which the following chemical and isotopic analyses will be carried out, X-ray powder diffraction (XRD) analyses were performed at INGV-OV. The X'Pert Powder diffractometer by Malvern-PANalytical was used. The diffractometer in the conventional Bragg-Brentano setup is equipped with a high-speed PIXcel detector. Analyses were performed by using Ni-filtered $\text{CuK}\alpha$ radiation, pyrolytic graphite crystal monochromator, at 40 kV and 40 mA in a $3\text{--}70^\circ 2\theta$ range with 0.02° steps at 8 s/step. Obtained diffraction patterns were interpreted using the X'Pert HIGH Score Plus computer program and JCPDS PDF-2 database. The semi-quantitative determination of the mineralogical composition of the investigated samples was carried out by using a X'pert HighScore Plus software, version 4.9.

5.5. $^{40}\text{Ar}/^{39}\text{Ar}$ analyses

The separation of alkali feldspars (grain-size in the range of 0.50–0.25 mm) from samples PR45.8–45.9 (PU-29) and PR99.5–99.6 (PU-1) was achieved by standard separation techniques and hand-picking under a stereomicroscope at the INGV-OV. $^{40}\text{Ar}/^{39}\text{Ar}$ analyses were performed at IGG-CNR (Pisa). The mineral separates were leached in an ultrasonic bath at room temperature for a few minutes in diluted HF (7 %) and were then wrapped in aluminium foil and irradiated (PAV-91, January 2023) for 3 h in the core of the TRIGA reactor at the University of Pavia (Italy) along with the reference mineral Alder Creek sanidine (ACs). A full replicate of sample PR99.5–99.6 was completed at a later time through a second irradiation of the same duration (PAV-94, April 2024) and using the same reactor as above. Grains of alkali feldspar were placed into 1.5-mm diameter holes, mostly individual grains but up to three grains in some cases (Table S1 in Supplementary Material), loaded into a vacuum chamber comprising a laser port consisting of a ZnSe window fitted with a differentially pumped flange and baked for 12 h at 150°C . Total fusion experiments were performed using a CO_2 laser beam (New Wave Research MIR10–30) defocused to a 0.8-mm spot. For sample PR45.8–45.9, a single step-heating experiment was completed on a larger grain, placed into a 3-mm diameter hole, using the same laser system as above, defocused to a 2-mm spot. Steps were carried out at increasing laser power until complete melting. Extracted gases were purified in a low volume stainless steel inlet system for 4 min (including 30 s of laser) using three SAES NP10 getters (one, water-cooled, held at $\sim 400^\circ\text{C}$ and two at room temperature). Ar isotope measurements were performed simultaneously in static mode using an ARGUS VI (Thermo Fisher Scientific) multicollector noble gas mass spectrometer. ^{36}Ar was measured using a Compact Discrete Dynode (CDD) detector and the remaining Ar isotopes (^{40}Ar , ^{39}Ar , ^{38}Ar and ^{37}Ar) using Faraday detectors equipped with $10^{13}\ \Omega$ resistors. Blanks were monitored generally every two runs and were subtracted from succeeding sample results (Table S1 in Supplementary Material). Uncertainty on the error-weighted mean ages also includes the uncertainty in the fluence monitor and is given at 2σ . Ages were calculated relative to an ACs age of 1.1848 Ma (Niespolo et al., 2017), using decay constants recalculated by Min et al. (2000) and an atmospheric $^{40}\text{Ar}/^{36}\text{Ar}$ ratio of 298.56 ± 0.31 (Lee et al., 2006). Ar isotope concentrations are reported in Supplementary Material (Table S1) as relative abundances, corrected for blank, mass discrimination, and radioactive decay. More details about mass spectrometer calibration and analysis can be found in Di Vincenzo et al. (2021) and Di Vincenzo (2022).

6. Results

6.1. General stratigraphy of the Ponti Rossi borehole

The general stratigraphy of the Ponti Rossi borehole is fully composed of pyroclastic deposits arranged in thirty-one PUs based on the adopted stratigraphic criteria (Fig. 4). Details about the depth interval, thickness, structural/textural characteristics, lithological

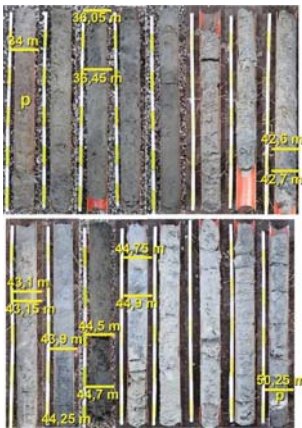
Table 1

Stratigraphy of the Ponti Rossi borehole. The interval of depth, thickness, description, lithological features of the juvenile fragments and emplacement mechanisms are reported for each Pyroclastic Unit (PU). For units formed by both pyroclastic current (PC) and fall (F) deposits, the main emplacement mechanism is reported first; (?) uncertain attribution.

Label	Interval of depth below the ground (m)	Thickness (m)	Description	Lithology and textural features of juvenile fragments	Depositional mechanisms	Photo (g.l. = ground level; p = paleosol; ~ erosional surface)
	0–2.50	2.5	Anthropogenic deposits			
PU-31 (NYT)	2.50–25.15	22.65	Massive to faintly laminated, light grey ash containing abundant rounded, well vesiculated, grey pumice lapilli. It grades upward in a 50 cm thick paleosol.	Light grey, slightly porphyric pumice	PC	
	25.15–26.70	1.55	Massive, coarse ash to medium lapilli deposit. In grades upward in a 0.08 m thick brown paleosol. Lithic clasts are very scarce and composed of lava.	Dark grey to blackish, moderately to well vesiculated, sub-aphyric scoria	F (?)	
	26.70–26.90	0.20	Massive, yellowish, coarse to fine ash with sub-angular to sub-rounded lapilli dispersed. Lapilli show a thin yellowish ash coating. Very rare obsidian. Lithic clasts are subordinate and composed of lava.	Well vesiculated, aphyric to sub-aphyric, light grey pumice Rare dark grey scoria	PC	
	26.90–27.70	0.80	Massive, dark grey, coarse to fine ash with abundant lapilli dispersed. Lithic clasts are abundant and composed of lava.	Light to dark grey, well vesiculated, slightly porphyric pumice	PC	
PU-30	27.70–28.70	1.0	Massive, grey to yellowish, coarse ash with abundant sub-rounded fine lapilli. Lithic clasts are very scarce and composed of lava.	Light grey, well vesiculated, sub-aphyric pumice Sporadic, micro-vesiculated, darker juvenile	PC (?)	
	28.70–29.20	0.50	Massive, coarse ash deposit rich in lithic fraction (62 wt%), composed of lava fragments, and a minor juvenile fraction made up of sub-angular to sub-rounded fine lapilli.	Light grey, slightly porphyric pumice	Reworked (?)	
	29.20–29.80	0.60	Massive, grey, coarse to fine ash with sub-angular to sub-rounded lapilli dispersed. Lithic clasts are very scarce and composed of lava.	Light grey, moderately to well vesiculated, slightly porphyric pumice	PC	
	29.80–31.75	1.95	Grey to yellowish, fine to coarse ash with fine lapilli dispersed. The structure varies from massive at the base to stratified at the top. The stratification is given by alternation of cm-thick horizons of fine ash and ash with sub-rounded lapilli dispersed. The uppermost part is brownish. Rare obsidian. Lithic clasts are very scarce and composed of lava	Light grey, micro-vesiculated, aphyric pumice Rare dark grey scoria	PC	
	31.75–31.90	0.15	Massive, clast-supported horizon consisting of angular, fine to medium lapilli. Lithic clasts are scarce and composed of lava.	Light grey, highly vesiculated, aphyric to slightly porphyric pumice. Rare darker pumice.	F	
	31.90–32.20	0.30	Massive ash with a few fine lapilli dispersed. It varies from grey at the base to yellowish at the top.	Light grey, aphyric to slightly porphyric pumice	PC	

(continued on next page)

Table 1 (continued)

Label	Interval of depth below the ground (m)	Thickness (m)	Description	Lithology and textural features of juvenile fragments	Depositional mechanisms	Photo (g.l. = ground level; p = paleosol; ~ erosional surface)
PU-29	32.20–34.00	1.80	Faintly stratified, fine to coarse ash with fine sub-rounded lapilli dispersed. Lithic clasts, made up of lava fragments, are very scarce at the top and increase toward the base.	Light grey, highly vesiculated, aphyric to slightly porphyric pumice. Rare dark grey, moderately vesiculated scoria.	PC	
	34.0–36.05	2.05	Massive, grey, coarse to fine ash with abundant, sub-rounded, coarse to fine lapilli. It grades in a 50 cm thick, brown paleosol containing light grey pumice fragments.			
	36.05–36.45	0.4	Lithic clasts are very scarce and composed of mm-sized lava fragments Reworked sandy layer Stratified deposit. Decimetre to metre thick, coarse to fine ash layers, with abundant, sub-rounded, fine to coarse lapilli and rare obsidian clasts, and fine ash layers with accretionary lapilli.	colluvial		
	36.45–42.6	6.15	Lithic clasts are scarce and composed of lava fragments and rare syenite.	PC		
	42.6–42.7	0.1	Reworked sandy layer	colluvial		
	42.7–43.1	0.4	Massive, grey ash deposit with a few, sub-rounded, coarse to fine lapilli dispersed.	PC		
	43.1–43.15	0.05	Lithic clasts are subordinate and composed of lava fragments. Reworked sandy layer	colluvial		
	43.15–43.9	0.75	Massive, grey ash deposit with a few, sub-rounded, coarse to fine lapilli dispersed and rare obsidians.	PC		
	43.9–44.25	0.35	Lithic clasts are scarce and composed of lava fragments. Reworked sandy layer	colluvial		
	44.25–44.5	0.25	Massive, grey, coarse to fine ash with abundant, sub-rounded, fine lapilli and rare obsidian clasts.	PC		
	44.5–44.7 m	0.2	Lithic are abundant and composed of mm-sized lava fragments and rare skarn Reworked sandy layer	colluvial		
	44.7–44.75	0.05	Massive, lithic-rich, grey ash deposit with a few fine lapilli dispersed.	PC		
	44.75–44.9	0.15	Lithics are predominantly composed of lava, very minor obsidian and rare skarn. Reworked sandy layer	colluvial		
	44.9–50.25	5.35	Faintly stratified, grey ash, with a variable amount of sub-rounded, coarse to fine lapilli dispersed and rare obsidian clasts. Lithic fragments are subordinate and composed of lava and rare syenite and skarn.	PC		

(continued on next page)

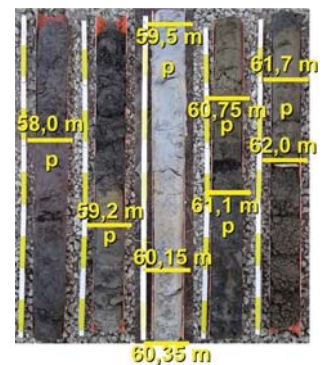
Table 1 (continued)

Label	Interval of depth below the ground (m)	Thickness (m)	Description	Lithology and textural features of juvenile fragments	Depositional mechanisms	Photo (g.l. = ground level; p = paleosol; ~ erosional surface)
PU-28	50.25–50.5	0.25	Thinly laminated, 10 cm thick, fine to medium, dark grey ash overlaid by a massive, light grey-whitish, 5 cm thick, fine ash with a few very fine, sub-angular, lapilli dispersed. It grades in a 10 cm thick, brown paleosol. Lithic clasts are abundant and predominantly composed of lava and rare skarn.	Base: grey, micro-vesiculated, aphyric to sub-aphyric pumice. Top: light grey, micro-vesiculated, aphyric pumice. Loose microcrysts of feldspar, pyroxene, black mica. Rare leucite at the base of the unit.	PC (?)	
PU-27	50.5–50.8	0.3	Massive, yellow-ochre, 20 cm thick, medium to fine ash, with scattered fine, rounded, pumice lapilli dispersed. It grades in a 10 cm thick, brown paleosol. Lithic clasts are abundant and completely composed of lava fragments	Predominantly, light grey, well-vesiculated, porphyritic pumice with microphenocrysts of pyroxene. Very subordinate dark grey, micro-vesiculated, aphyric pumice. Loose microcrysts of feldspars, pyroxene and black mica.	PC	
PU-26	50.8–51.35	0.55	Massive, 25 cm thick, coarse ash to very fine lapilli deposit with rare obsidian clasts and extremely rich in lithic fragments (91 wt%). Lithic clasts are composed of lava and very rare syenite. Very minor juvenile fragments mostly composed of altered pumice clasts. The upper 30 cm are thinly laminated and humified.	Grey, micro-vesiculated, aphyric, pumice. Loose crystals of feldspar, pyroxene, black mica, leucite and opaque oxide.	Reworked volcanoclastic unit	
PU-25	51.35–51.8	0.45	Massive, 15 cm thick, grain-supported deposit composed of angular, fine to medium lapilli. It grades in a 30 cm thick paleosol changing upward in colour from dark brown to ochre. Lithic clasts are very subordinate and composed of lava fragments.	Light grey, micro-vesiculated, porphyritic to sub-aphyric pumice with phenocrysts of feldspar and microcrysts of pyroxene and black mica. Very rare dark grey pumice. High amount of loose feldspar, pyroxene and black mica.	F	
PU-24	51.8–52.1	0.3	Faintly stratified and humified ash	Grey, micro-vesiculated, slightly porphyritic pumice. Very rare, dense scoria and obsidian clasts.	PC (?)	
PU-23	52.1–52.9	0.8	Massive, 20 cm thick, medium to fine ash with a few fine, sub-rounded lapilli dispersed. It grades upward in a light brown-greyish, 60 cm thick paleosol. Lithic clasts are subordinate and composed of lava and rare syenite fragments.	Loose crystals of pyroxene, feldspar and black mica.	PC	
PU-22	52.9–53.05	0.15	Massive, 10 cm thick, yellowish ash with a few sub-rounded, fine lapilli dispersed. It grades upward in a 5 cm thick, brown paleosol. Lithic clasts are scarce and composed of lava fragments	Dark grey, micro-vesiculated, aphyric to slightly porphyritic pumice with pyroxene microcrysts. Very rare light grey pumice. Loose crystals of pyroxene, feldspar and black mica.	PC	
PU-21	53.05–53.18	0.13	Massive, 8 cm thick, coarse to fine ash with a few fine, sub-rounded, lapilli dispersed. It grades in a 5 cm thick, light brown paleosol. Lithic clasts are subordinate and composed of lava and rare syenite fragments.	Dark grey, micro-vesiculated, aphyric to slightly porphyritic pumice with black mica phenocrysts. Light grey, micro-vesiculated, slightly porphyritic pumice are subordinate. Loose crystals of pyroxene feldspar, black mica, leucite and opaque oxide.	PC (?)	
PU-20	53.18–53.68	0.5	Massive, 18 cm thick, yellowish ash with abundant, rounded, fine to medium lapilli dispersed. It grades in a 32 cm thick brown paleosol. Lithic fragments are scarce and	Light grey, aphyric to sub-aphyric, well vesiculated pumice with circular vesicles and phenocrysts of feldspar, black mica and pyroxene. Loose crystals of feldspar and	PC	

(continued on next page)

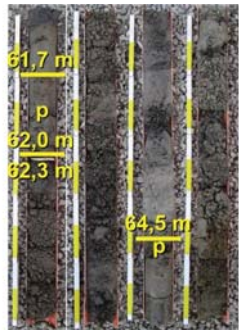
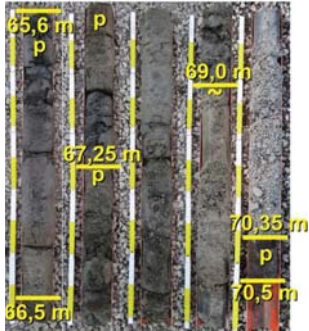
Table 1 (continued)

Label	Interval of depth below the ground (m)	Thickness (m)	Description	Lithology and textural features of juvenile fragments	Depositional mechanisms	Photo (g.l. = ground level; p = paleosol; ~ erosional surface)
PU-19	53.68–58.0	4.32	mainly composed of lava and very rare syenite and skarn. Stratified unit made up of decimetre- to metre-thick layers. Alternating of thick, matrix-supported, grey, coarse to fine ash layers with abundant, rounded to sub-rounded, fine to coarse lapilli, and thinner grain-supported layers of angular, medium to coarse lapilli. The deposit became darker upward and grades in a 20 cm thick, light brown paleosol. Very rare obsidian. Lithic clasts are abundant throughout the sequence and predominantly composed of lava and very rare syenite and skarn.	subordinate pyroxene, black mica and opaque oxide. Predominantly, light grey, slightly porphyritic, well-vesiculated pumice with phenocrysts of pyroxene, feldspar and black mica. Vesicle shape ranges from circular to tubular. Coarse pumice clasts bear mm-sized lava fragments, and some pumice clasts show an orange patina. Dark grey, slightly porphyritic, micro-vesiculated pumice are very subordinate.	PC/F	
PU-18	58.0–59.2	1.2	Massive to faintly laminated, 10 cm thick, yellow-ochre, fine ash covered by a 90 cm thick, grey deposit composed of angular to sub-angular, fine to coarse lapilli. It grades upward in a 20 cm thick, brown paleosol. Lithic fragments are subordinate and mainly composed of porphyritic leucite-bearing lava and very rare syenite.	Loose crystals of pyroxene and subordinate feldspar, black mica, leucite and opaque oxide. Grey, well vesiculated, slightly porphyritic pumice with phenocrysts of feldspar and subordinate black mica and pyroxene. Some pumice clasts show a silky texture. Dark grey to blackish, denser, micro-vesiculated pumice are subordinate.	F/PC	
PU-17	59.2–59.5	0.3	Massive, 20 cm thick, grey, coarse to fine ash deposit. It became slightly darker upward. Fine, sub-rounded lapilli are dispersed. It grades upward in 10 cm thick brownish paleosol. Lithic clasts are scarce and composed of lava fragments.	Loose crystals of pyroxene and subordinate feldspar, black mica, leucite and opaque oxide. Grey, vesiculated, aphyric to sub-aphyric pumice with rare microcrysts of pyroxene and black mica. Some pumice clasts show a silky texture. Rare, dark grey, micro-vesiculated pumice.	PC	
PU-16	59.5–60.15	0.65	Massive, 15 cm thick, brownish to ochraceous, coarse to fine ash deposit with sub-rounded, fine lapilli. It grades upward in a 50 cm thick, greyish to brownish paleosol. Lithic clasts are subordinate and composed of lava and rare syenite fragments.	Loose crystals of pyroxene, feldspar, black mica, leucite and opaque oxide. Grey, micro-vesiculated, slightly porphyritic pumice with pyroxene and feldspar phenocrysts. Rare, denser, dark scoria. Loose microcrysts of pyroxene, feldspar, black mica, leucite and opaque oxide.	PC	
PU-15	60.15–60.35	0.2	Massive, 15 cm thick, brownish, coarse to fine ash with sub-rounded, fine to medium lapilli dispersed. It grades upward in a 5 cm thick light brown paleosol. Lithic clasts are subordinate and composed of leucite-bearing lava and rare syenite fragments.	Grey, micro-vesiculated, slightly porphyritic pumice with pyroxene, analcime/leucite and feldspar phenocrysts. Coarser clasts bear sub-mm-sized lava fragments. Loose microcrysts of pyroxene, feldspar, black mica, analcime/leucite and opaque oxide.	PC	
PU-14	60.35–60.75	0.4	Massive, 20 cm thick, grey to yellowish ash with rounded fine lapilli dispersed. It grades upward in 20 cm thick, light brown to greyish paleosol. Lithic clasts are subordinate and composed of leucite-bearing lava and very rare syenite.	Grey, micro-vesiculated, slightly porphyritic pumice with feldspar, black mica, analcime/leucite and pyroxene phenocrysts. Rare, denser, dark grey scoria. Loose crystals of feldspar, pyroxene, black mica and analcime/leucite.	PC	
PU-13	60.75–61.1	0.35	Massive, 10 cm thick, grey, coarse to fine ash deposit with	Light grey, vesiculated, slightly porphyritic pumice with	PC	



(continued on next page)

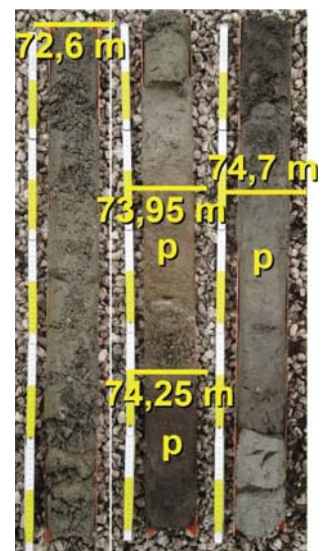
Table 1 (continued)

Label	Interval of depth below the ground (m)	Thickness (m)	Description	Lithology and textural features of juvenile fragments	Depositional mechanisms	Photo (g.l. = ground level; p = paleosol; ~ erosional surface)
			sub-rounded fine to medium lapilli dispersed. It grades upward in a 25 cm thick, brown paleosol. Lithic clasts are abundant and composed mainly of aphyric to porphyritic leucite-bearing lava and rare skarn and syenite fragments.	pyroxene, black mica, leucite and feldspar phenocrysts. Some pumice clasts show a silky texture. Dark grey, micro-vesiculated, slightly porphyritic scoria clasts are very subordinate. Loose crystals of pyroxene, black mica, feldspar and subordinate olivine, leucite and opaque oxide.		
PU-12	61.1–61.7	0.6	Massive to faintly laminated, 50 cm thick, yellow-ochre fine ash deposits with sporadic accretionary lapilli and a few very fine lapilli. It grades upward in a 10 cm thick, brownish to greyish paleosol. Lithic clasts are abundant and composed of lava fragments.	Grey, micro-vesiculated, slightly porphyritic pumice with pyroxene, black mica and feldspar phenocrysts. Loose crystals of pyroxene, black mica, feldspar and rare opaque oxide and analcime/leucite.	PC	
	61.7–62.0	0.3	Light brown paleosol			
	62.0–62.3	0.3	Material lost during drilling operations			
PU-11	62.3–64.5	2.2	Stratified unit made up of decimetre- to metre-thick layers. Alternating of thick, grain-supported layers consisting of angular, coarse lapilli and much thinner matrix-supported, grey, fine ash layers with abundant, rounded to sub-rounded, fine to coarse lapilli. Single layers are massive with no internal stratification. Matrix-supported layers occur toward the base of the unit. The top was truncated during drilling operations and part of the material was lost. Very rare obsidian. Lithic clasts are abundant, increasing toward the base, and composed of fresh and hydrothermalized lava fragments, skarn and syenite clasts.	Light grey, highly vesiculated, slightly porphyritic pumice with feldspar and subordinate pyroxene and black mica microcrysts. Circular to stretched vesicles. Darker and slightly denser, slightly porphyritic pumice clasts are subordinate. Loose crystals of pyroxene, black mica and feldspar.	F/PC	
			Massive to faintly stratified, 85 cm thick, grain-supported deposit composed of angular, coarse to medium lapilli covered by a 20 cm thick, grey to yellowish ash with abundant sub-rounded lapilli dispersed. It grades upward in a 5 cm thick paleosol. Lithic clasts are subordinate and composed of fresh and hydrothermalized lava and rare syenite fragments.	Light grey, highly vesiculated, slightly porphyritic pumice with crystals of feldspar, pyroxene and black mica. Vesicle shape is mainly circular and sub-mm in size. Sporadic, denser and darker and micro-vesiculated pumice. Loose crystals of pyroxene, black mica, feldspar and opaque oxide.	F/PC	
PU-10	64.5–65.6	1.1	Massive, 55 cm thick, grey to yellowish, lithic-rich, coarse to fine ash deposit with rounded, fine lapilli dispersed. It became finer grained and faintly laminated upward. It is covered by a 35 cm thick, reworked and humified sandy deposit. Lithic fraction is composed of lava fragments and rare skarn and syenite clasts	Grey, micro-vesiculated, aphyric to sub-aphyric pumice with pyroxene microcrysts. Loose crystals of pyroxene, feldspar and black mica.	PC	
PU-9	65.6–66.5	0.9	Massive, 25 cm thick, coarse ash to fine lapilli deposit with scarce matrix and extremely rich in lithic fragments (95 wt%)	Grey, micro-vesiculated, porphyritic pumice with feldspar phenocrysts. Dark grey, denser scoria clasts	Reworked volcanoclastic unit	

(continued on next page)


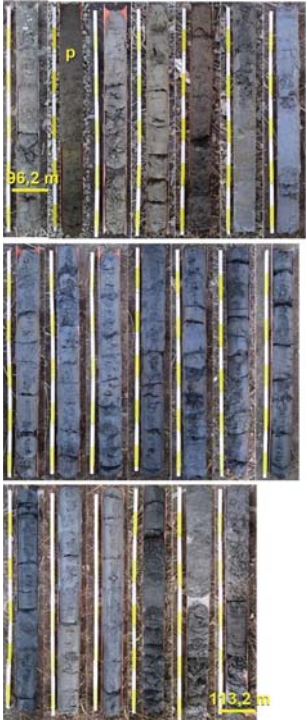
Table 1 (continued)

Label	Interval of depth below the ground (m)	Thickness (m)	Description	Lithology and textural features of juvenile fragments	Depositional mechanisms	Photo (g.l. = ground level; p = paleosol; ~ erosional surface)
PU-7	67.25–69	1.75	composed predominantly of lava and very rare syenite and skarn. The juvenile fraction is very low and composed of altered pumice and scoria clasts. It grades upward in a 50 cm thick paleosol.	with pyroxene and black mica phenocrysts.	F/PC	
			Four superimposed stratigraphic units, from the base upward: 60 cm thick, matrix-poor to grain-supported deposit composed of angular to sub-angular, fine to coarse pumice lapilli.	Loose crystals of pyroxene, feldspar, black mica and rare leucite.		
			50 cm thick, laminated fine ash with accretionary lapilli.	Light to dark grey, micro-vesiculated, aphyric to slightly porphyritic pumice with feldspar crystals. Some pumice clasts show a silky texture.		
			55 cm thick deposit having the same characteristics of the base. 10 cm thick, massive, grey ash with sub-rounded fine lapilli dispersed. The top is humified. Lithic clasts are abundant in both ash and lapilli layers and composed of lava fragments and skarn.	Dark grey to blackish, dense, sub-aphyric scoria.		
PU-6	69.0–70.35	1.35	Massive, 60 cm thick, grain-supported deposit composed of angular, coarse lapilli overlaid by a matrix-supported, grey to yellowish ash deposit, 75 cm thick, with abundant, sub-rounded, fine to coarse lapilli. At the top an erosional surface. Lithic clasts are scarce and composed of lava fragments	Loose crystals of feldspar and subordinate pyroxene, leucite and black mica.	PC/F	
			Dark brown paleosol	Light grey, highly vesiculated, slightly porphyritic pumice with feldspar and pyroxene phenocrysts. Some pumice clasts have an orange superficial patina.		
			Material lost during drilling operations	Dark grey, dense, porphyritic scoria, with feldspar phenocrysts, are rare.		
PU-5	70.35–70.5	0.15			F/PC	
	70.5–72.6	2.1	Massive, 25 cm thick, light grey fine ash, with a few fine lapilli dispersed, covered by a 110 cm thick deposit composed of sub-angular, medium to fine lapilli with a very scarce, coarse ash matrix. The top was truncated during drilling operations and part of the material was lost. Lithic clasts are abundant and composed of lava fragments.	Loose crystals of pyroxene, feldspar, black mica and opaque oxide.		
PU-4	72.6–73.95	1.35	Massive, 15 cm thick deposit made up of angular, medium to fine lapilli with a very scarce ash matrix. It grades upward in a 15 cm thick paleosol. Lithic clasts are abundant and composed of lava fragments.	Light grey, well vesiculated, aphyric to sub-aphyric pumice with pyroxene microcrysts. Dense, aphyric to sub-aphyric scoria are rare.	F	
				Loose crystals of pyroxene and feldspar.		
PU-3	73.95–74.25	0.3	Massive, 20 cm thick deposit composed of angular, medium to fine lapilli with a very scarce ash matrix. It grades upward in a 15 cm thick paleosol. Lithic clasts are abundant and composed of lava fragments.	Light grey, well-vesiculated, aphyric to sub-aphyric pumice with sporadic feldspar microcrysts.	F	
				Loose crystals of pyroxene, feldspar, black mica and opaque oxide.		
PU-3	74.25–74.7	0.45	Massive, 20 cm thick, grain-supported deposit composed of coarse ash to angular fine lapilli. It grades upward in a 25 cm thick paleosol. Lithic clasts are abundant and composed of lava fragments and a few syenite clasts.	Light grey, well-vesiculated, slightly porphyritic pumice with pyroxene and black mica microcrysts.	F	
				Rare, denser, slightly porphyritic scoria clasts.		
PU-3	74.25–74.7	0.45		Loose crystals of pyroxene, feldspar, black mica and opaque oxide.	F	



(continued on next page)

Table 1 (continued)

Label	Interval of depth below the ground (m)	Thickness (m)	Description	Lithology and textural features of juvenile fragments	Depositional mechanisms	Photo (g.l. = ground level; p = paleosol; ~ erosional surface)
PU-2	74.7–96.2 m	21.5	<p>Stratified unit. Alternating of meter-thick ash layers containing abundant rounded, light to dark grey, fine to coarse lapilli and fine ash layers rich in accretionary lapilli. Single layers are massive with no internal stratification. The deposit became darker upward and grades in a 30 cm thick paleosol. At c. 75.7 m of depth, a 10 cm thick, matrix-poor, lithic- and scoria-rich reworked horizon occurs. Rare obsidian. Lithic fragments are subordinate and composed of lava. Two lava fragments, at c. 87 m of depth, 6.5 cm in diameter, possibly emplaced as ballistics, have been found.</p> <p>Base not reached. At the base, a 13.55 m thick, roughly stratified, matrix-poor deposit composed of coarse scoriaceous ash with abundant, sub-rounded to sub-angular, coarse to fine scoria lapilli covered by a 2.05 m thick, massive, matrix-poor deposit, composed of coarse ash with abundant coarse to fine, sub-rounded, pumice lapilli. It is capped by a 20 cm thick, faintly laminated, grey to yellowish ash deposit with accretionary lapilli. It grades upward in a 90 cm thick, brown paleosol in turn covered by a 30 cm thick, reworked and humified sandy deposits. Rare obsidian. The amount of lithic clasts is variable being abundant at the base and top of the sequence and scarce in the middle part. Lithic clasts are predominantly composed of fresh and hydrothermally altered lava, sporadic skarn and mm-sized hydrothermally altered tuffs. Toward the base of the unit, sporadic fragments of sedimentary nature (siltite) have been found. Free crystals are abundant throughout the unit, particularly toward the base of the scoriaceous part.</p>	<p>Light to dark grey, well-vesiculated, slightly porphyritic pumice with feldspar and black mica phenocrysts.</p> <p>Loose crystals of feldspar, black mica and pyroxene.</p>	PC	
PU-1	96.2–113.2	>17.0	<p>Blackish, moderately vesiculated, porphyritic scoria with feldspar phenocrysts. Grey, well vesiculated to micro-vesiculated, slightly porphyritic pumice with pyroxene and black mica microcrysts. Loose crystals of feldspar and subordinate pyroxene, black mica and opaque oxide.</p>	PC		

features of the juvenile/lithic fragments and emplacement mechanisms of each PU are reported in Table 1. PUs are labelled progressively with an alphanumeric code from the deepest and oldest (PU-1) to the shallowest and youngest one (PU-31). The thickness of the PUs ranges from 22.65 m (PU-31) to 13 cm (PU-21). The PUs are always separated by paleosols or humified reworked materials, except for PU-6 and PU-7 which appear to be separated by an erosional surface (Fig. 5a). PU-29

features six centimetre- to decimetre-thick, lithic-rich, reworked sandy layers (Table 1) with no evidence of pedogenesis/humification so, according to our stratigraphic criteria, they are not considered as bounding surfaces of different units. Paleosols are sandy to silty, between 5 and 90 cm thick, and characterized by different degrees of maturity. They vary from very mature and dark brown in colour to less mature and light brown in colour. Some paleosols grade from dark brown at the top to

Table 2
Semi-quantitative X-Ray Diffraction analysis of the selected samples. All concentrations are in wt%.

Sample	Feldspar	Biotite	Analcime	Leucite	Olivine	Pyroxene	Quartz
PR22.55–22.60	78.3	7.0		14.7			
PR26.75–26.80	81.0	1.6		2.4		15.0	
PR27.6–27.65	89.9	0.8		0.2		9.1	
PR28.0–28.1	74.2	8.7				17.1	
PR28.9–29.0	78.0	2.0		8.0		12.0	
PR29.50–29.55	94.8	2.6		2.6			
PR33.2–33.3	81.2	15.1				3.7	
PR35.5–35.6	68.5	28.7				2.8	
PR43.5–43.6	51.5	38.5				10.0	
PR49.5–49.6	85.3	5.6				9.1	
PR50.35–50.40	76.1	3.2		1.0		19.7	
PR50.45–50.5	52.3					47.7	
PR50.6–50.7	71.1	27.5				1.4	
PR51.2–51.3	66.2	1.0		1.7		31.1	
PR51.70–51.75	68.8	29.5				1.7	
PR52.85–52.90	92.2	2.4				5.4	
PR52.95–53.0	84.1	3.8		4.5		7.6	
PR53.10–53.15	75.6	3.5		4.3		16.6	
PR53.55–53.65	47.5	30.4				22.1	
PR56.8–56.9	73.4	0.7		21.3		4.6	
PR58.9–59.0	65.4	3.1		19.7		11.8	
PR59.35–59.40	72.6	1.6		12.1		13.7	
PR59.45–59.50	85.4	0.6		6.8		7.2	
PR60.05–60.15	77.8	5.8	9.1			7.3	
PR60.25–60.35	74.0	10.9	10.1			5.0	
PR60.6–60.7	78.3	3.9	5.7			12.1	
PR61.0–61.1	69.2	12.2		6.2		12.4	
PR61.5–61.6	75.8	14.1		5.9		4.2	
PR64.15–64.25	89.2	0.8		4.3		5.7	
PR65.2–65.3	86.9	0.7		6.5	2.0	3.9	
PR66.3–66.4	72.8	2.3		7.2	1.2	16.5	
PR67.1–67.2	83.1	1.6		7.5		7.8	
PR67.25–67.35	84.8	3.0		6.1		6.1	
PR68.7–68.8	72.7	5.5		1.0		20.8	
PR70.15–70.25	89.8	3.5				6.7	
PR73.5–73.6	84.1	11.4				4.5	
PR74.1–74.2	85.8	6.0				8.2	
PR74.5–74.6	78.7	9.4				11.9	
PR75.1–75.2	70.5	17.1				12.4	
PR95.9–96.0	86.1	1.3				12.6	
PR97.4–97.5	77.6	9.7				12.7	7.9
PR98.20–98.45	96.6	2.0				1.4	
PR112.9–113.0	95.4	1.7				2.9	

light brown-yellowish at the base and often contain juvenile fragments. Pyroclastic deposits vary from grain-supported beds of angular, coarse to fine lapilli to matrix-supported coarse to fine ash deposits, locally rich in accretionary lapilli, with a variable amount of rounded to sub-rounded lapilli dispersed into the matrix. Matrix-supported ash deposits vary from massive to faintly stratified/laminated due to internal grain size variation. From a lithological point of view, the juvenile fraction is characterized by the coexistence, in some units, of different juvenile types differentiated on the basis of vesicularity degree, vesicle size and colour (Fig. 6). Juvenile fragments are composed of both light to dark grey pumice and blackish, denser scoria. Their texture varies from highly vesiculated, with circular to stretched vesicles, to micro-vesiculated to silky. Moreover, the juvenile fragments are both aphyric to slightly porphyritic with feldspar, pyroxene, biotite and, in a few cases, leucite (Fig. 6). Obsidian has been also recognised in some units (Fig. 6). Lithic clasts are predominantly composed of fresh and hydrothermally altered lava and very minor skarn, syenite and altered tuff fragments. Fragments of sedimentary rocks (siltite) were only found at the base of the lowermost cored unit (PU-1). Peculiar leucite-bearing lava and scoria fragments characterize some units. The different types of lithic fragments of primary and reworked volcanoclastic deposits are shown in Fig. 6. Pyroclastic deposits, irrespective of the emplacement mechanisms, show great variability in lithology and abundance of both juvenile and lithic fragments (Fig. 7).

The sequence, from the base (113.2 m below the ground level)

upwards, is briefly described below focusing on relevant units. For the sake of simplicity, the cored succession can be subdivided into three parts (basal, middle, and upper; Fig. 4) that include PUs having similar thickness and/or lithological/structural characteristics.

6.1.1. Basal part

This part of the sequence (Fig. 4) is formed by the lowermost two units (PU-1 and PU-2) that total a thickness of 38.5 m (from 113.2 to 74.7 m) representing 34 % of the borehole length.

PU-1 is the lowermost cored unit whose base was not crossed. It has a minimum thickness of 17 m (113.2 to 96.2 m of depth). It can be divided into three layers based on different lithological/grain-size features and is the only unit, throughout the sequence, in which most of the thickness is characterized by scoriaceous clasts. The basal 13.55 m are faintly stratified due to grain-size variations and composed of coarse scoriaceous ash containing abundant, fine to coarse, sub-angular to sub-rounded scoria lapilli. Lithic clasts are abundant at the base (up to 82 wt%) and strongly diminish toward the top (5 wt%). They are predominantly composed of fresh and hydrothermally altered lava fragments. Sporadic lithic fragments of sedimentary nature (siltite, Fig. 6) and hydrothermally altered tuffs have been found. This scoriaceous part is covered by a 2.05-m-thick deposit composed of a massive, light grey, coarse to fine ash containing fine to coarse, sub-rounded, light grey pumice lapilli. Lithic fragments, predominantly composed of fresh and hydrothermally altered lava, increase upward passing from 10 to 57 wt

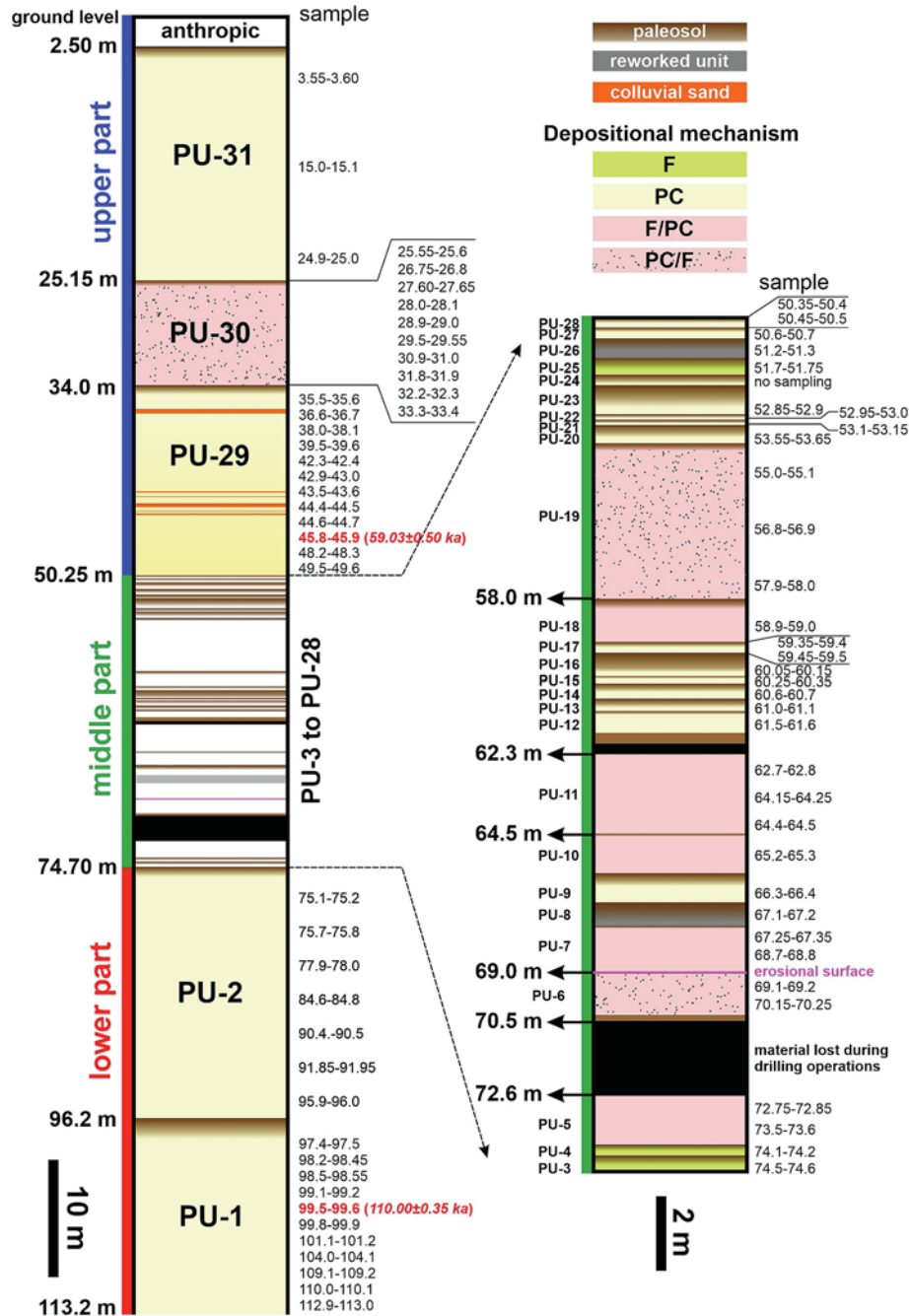


Fig. 4. Schematic log of the Ponti Rossi borehole arranged in three parts (lower, middle and upper) and thirty-one Pyroclastic Units (PU). A magnification of the middle part of the succession, due to the high number of very thin PUs, is reported to the right. The samples selected for $^{40}\text{Ar}/^{39}\text{Ar}$ analyses are highlighted in red (the age is reported in brackets). The depositional mechanism is reported for each unit: F = fall, PC = pyroclastic current. For units formed by both fall and pyroclastic current deposits, the main depositional mechanism is reported first. (For interpretation of the references to colour in this figure legend, the reader is referred to the web version of this article.)

%. It is capped by a faintly laminated, grey to yellowish, 20 cm thick, fine ash deposit with accretionary lapilli. It grades in a 90-cm-thick, brown paleosol in turn covered by a 30-cm-thick, reworked and humified sandy deposits.

PU-2 is 21.5 m thick (96.2 to 74.7 m of depth) and is the second thickest unit of the whole succession. This unit shows constant structural and lithologic features throughout its thickness. It is a roughly stratified deposit consisting of an alternating of ash layers containing abundant rounded, light to dark grey, fine to coarse pumice lapilli and finer ash layers rich in accretionary lapilli. Lithic abundance, almost completely composed of lava fragments, is very low at the top (<1 wt%) and slightly

increases downward (up to 14 wt%). Few scoriaceous clasts are dispersed. Two outsized lithic lava fragments, up to 6.5 cm in diameter (Fig. 5b), likely emplaced as ballistitic clasts, have been found at ~87 m of depth testifying to the relative closeness of the vent. At 75.7 m of depth, a <10 cm thick, lithic- and scoria-rich, matrix-poor, reworked horizon occurs.

6.1.2. Middle part

It comprises the interval between PU-3 and PU-28, from 74.7 to 50.25 m depth, and is the stratigraphically most complex portion being composed of 26 units totalling 24.45 m (21.6 % of the borehole length).

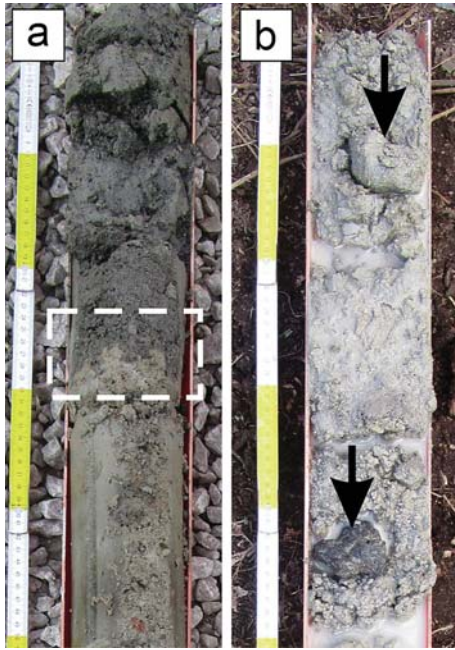


Fig. 5. a) Undulated sub-aerial erosional surface (highlighted by the white dashed rectangle) between PU-6 and PU-7; b) outsized lithic lava fragments in PU-2.

Three units (PU-3, PU-4 and PU-25) are centimetre- to a few decimetres-thick, massive, grain-supported deposits composed of fine pumice lapilli and subordinate lithic clasts. Lithic lava fragments are quite abundant in PU-3 (37 wt%) and scarce in PU-4 and PU-25 (~5 wt%). Seven units

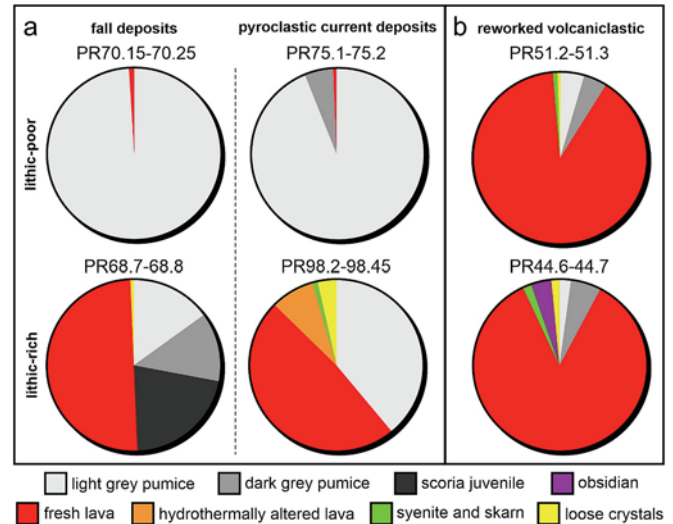


Fig. 7. Pie diagrams for componentry abundances of selected samples: a) primary pyroclastic deposits (both fallout and pyroclastic current) show a great variability in lithology and abundance of both lithic and juvenile fragments while b) reworked volcanoclastic deposits, including colluvial sands (PR44.6–44.7) from PU-29 are always extremely rich in lithic lava fragments and depleted in juvenile material.

(PU-5, PU-6, PU-7, PU-10, PU-11, PU-18 and PU-19) consist of meter-thick, layered deposits made up of massive to roughly stratified layers of grain-supported, medium to coarse pumice lapilli and massive, matrix-supported layers with abundant rounded to sub-rounded, coarse to fine pumice lapilli and a variable amount of lithic fragments. Fourteen units (PU-9, PU-12 to PU-17, PU-20 to PU-24, PU-27, PU-28) are formed

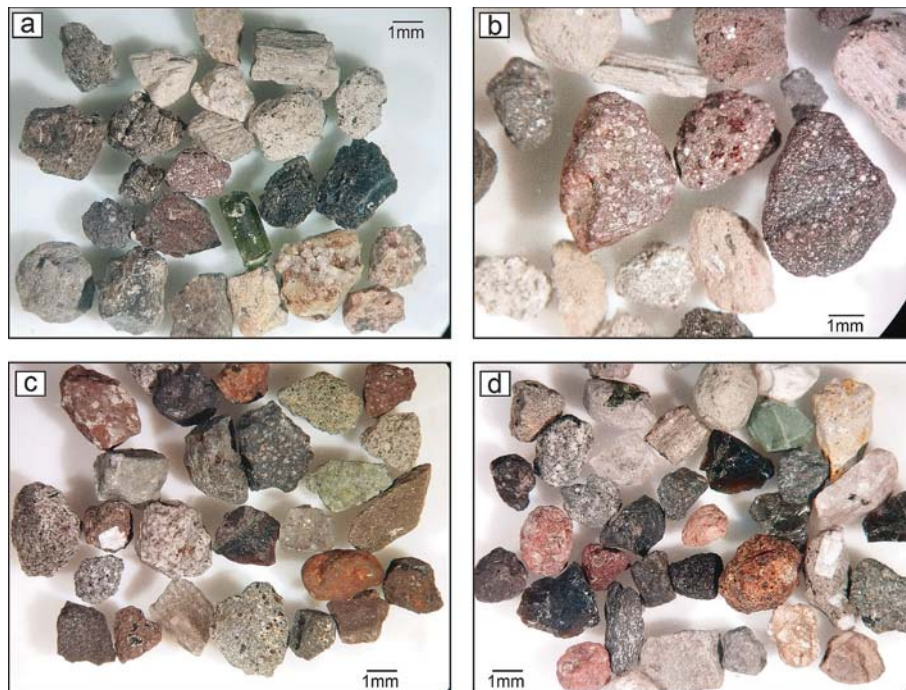


Fig. 6. Photos taken under a stereomicroscope showing the main lithological features of the cored sediments: a) coexistence of light to dark grey pumice and scoria juvenile, lithic fragments (lava, skarn and syenite) and a loose crystal of green pyroxene in sample PR68.7–68.8; pumice fragments show a variable degree of vesicularity and are either porphyritic or aphyric; b) leucite-bearing lithic lava fragments and juvenile clasts with leucite crystals in sample PR55.0–55.1; c) different types of lithic clasts (fresh and hydrothermally altered lava, syenite and skarn) including those of sedimentary nature (siltite) in sample PR112.9–113.0; d) lithic-rich colluvial sand (sample PR44.6–44.7) from PU-29 characterized by lithologically heterogeneous lithic clasts (fresh and altered lava, syenite and skarn), rounded juvenile fragments, obsidians and loose crystals of feldspar. (For interpretation of the references to colour in this figure legend, the reader is referred to the web version of this article.)

by centimetre- to decimetre-thick deposits consisting of massive to faintly laminated, grey to yellowish, fine to coarse ash with fine, rounded to sub-rounded pumice lapilli and subordinate lithic fragments. Fine-grained ash layers are locally rich in accretionary lapilli. PU-8 and PU-26 are massive, matrix-poor, volcanoclastic deposits extremely rich in mm-sized lithic fragments (>90 wt%), predominantly made up of lava (Fig. 7). The minor juvenile fraction is composed of altered and rounded pumice and scoria clasts (Fig. 6). It is worth noting that PU-13, PU-14, PU-15 and PU-18 are characterized by the presence of sub-mm-sized leucite-bearing lithic lava fragments (Fig. 6).

6.1.3. Upper part

The shallow interval of the sequence includes three PUs (PU-29 to PU-31) that total a thickness of 47.75 m plus 2.5 m (50.25 m to ground level) of anthropogenic deposits on top (44.4 % of the whole borehole length).

PU-29 is a 16.25-m-thick (from 50.25 to 34.0 m of depth) sequence formed by primary pyroclastic deposits intercalated by six, centimetre- to decimetre-thick, reworked, lithic-rich (Fig. 7), sandy layers. The presence of reworked (colluvial) sandy layers defines 7 sub-units in the PU-29 composed of massive to faintly stratified, matrix-supported, fine to coarse ash deposits with sub-rounded, grey pumice lapilli and fine ash layers with accretionary lapilli. The uppermost sub-unit grades upward in a 0.5-m-thick, brown paleosol containing grey pumice fragments.

PU-30 is 8.85 m thick (from 34.0 to 25.15 m) and can be subdivided into ten sub-units, ranging in thickness from 0.15 to 1.95 m, with no physical discontinuities between them apart from structural and lithological differences. Seven sub-units consist of grey to yellowish, fine to coarse ash with a variable amount of pumice lapilli. Three sub-units consist of clast-supported to matrix-poor coarse ash to (pumice or scoria) lapilli deposits. The uppermost sub-unit grades upward in a 0.08-m-thick brown paleosol underlying the topmost PU-31.

PU-31 is the thickest unit, being 22.65 m thick (from 25.15 to 2.5 m), and shows constant structural and lithological features throughout its thickness. It consists of a massive to faintly laminated, light grey ash containing abundant rounded slightly porphyritic, grey pumice lapilli, grading to a 0.5 m thick brown paleosol. It represents the shallowest cored volcanic sediments. This unit is capped by 2.5 m of anthropogenic deposits.

6.2. XRD analyses

XRD analyses, performed on 43 selected samples (Table 2), show a wide variability of crystallinity degree, amorphous content, and mineral

assemblage. The crystallinity degree (red line in Fig. 8) varies between 10 and 70 % and it has been obtained by normalized wt% based on the amorphous bend size. Most samples present a high percentage of amorphous phase, which may reflect the abundance of juvenile material. Conversely, the mineralogical assemblages reflect the content of loose crystals and of crystals contained in lithic and pumice fragments. In terms of XRD analyses, the most crystalline samples are PR27.60–27.65, PR33.30–33.40, PR35.50–35.60, PR43.50–43.60, PR60.25–60.35, PR67.25–67.35 and PR97.40–97.50. Conversely, the aphyric samples are PR22.55–22.60, PR28.00–28.10, PR60.60–60.70, PR70.15–70.25, PR73.50–73.60 and PR74.10–74.20. The mineralogy of the ϕ bulk fraction consists mainly of feldspars, pyroxene and biotite, whilst leucite, analcime and olivine locally occur. Quartz is present in a single sample (PR97.4–97.5) with 7.9 wt%. Feldspar dominates in the mineralogical assemblage even reaching values up to 96.6 wt%. The biotite content ranges from a minimum of 0.6 wt% to a maximum of 38.5 wt% (i.e., samples PR59.45–59.50 and PR43.50–43.60, respectively), although its detection is strongly influenced by the crystal orientation. Samples PR22.55–22.60 and PR29.50–29.55 are characterized by feldspar, biotite and leucite whilst the sample PR50.45–50.50 is characterized by feldspar and pyroxene crystals. Leucite is present in 21 samples shallower than 68.8 m depth, whereas analcime seems to be present only between 60.05 and 60.7 m.

Based on the sedimentological characterization of the Ponti Rossi samples (Table 1), most of the samples are constituted of at least 85 % of juvenile material. Therefore, the results of the XRD analyses in most of the cases can be ascribed to the magmatic component. In the other cases (PR50.35–50.40, PR50.45–50.50, PR56.80–56.90, PR58.90–59.00, PR61.00–61.10, PR61.50–61.60, PR64.15–64.25, PR67.10–67.20, PR67.25–67.35, PR74.50–74.60, PR98.20–98.45, PR112.90–113.00), they must be related to lithic fragments and loose crystals, which could be either ante/xenocrysts or phenocrysts and microlites.

6.3. $^{40}\text{Ar}/^{39}\text{Ar}$ data

Twenty-one out of twenty-four total fusion analyses (Table S1 in Supplementary Material) of alkali feldspars from sample PR45.8–45.9 (Fig. 9a), collected from the lowermost sub-unit of PU-29, yielded ages indistinguishable within analytical uncertainties (mean square of weighted deviates, MSWD = 1.36), with a weighted mean age of 59.03 ± 0.50 ka ($\pm 2\sigma$ internal uncertainty). Two total fusion analyses gave significantly older ages (Fig. 9a), with a mean of 65.3 ± 2.0 ka and are considered xenocrysts. A third discordant analysis gave a much younger age (20 ± 11 ka), but data are strongly contaminated by atmospheric Ar

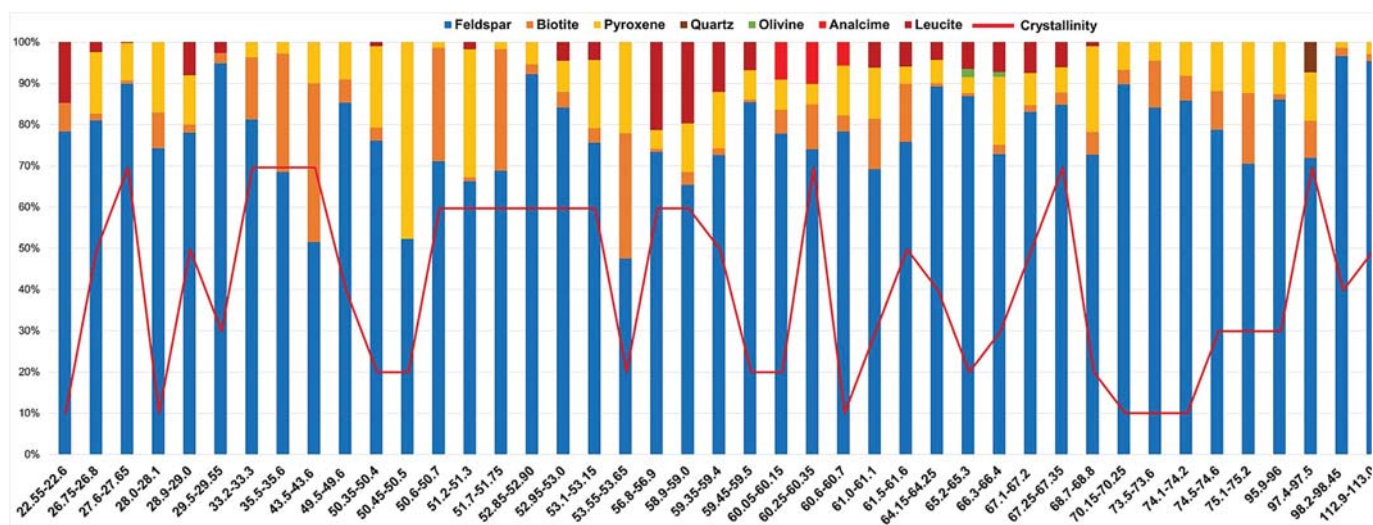


Fig. 8. Mineralogical assemblages and distribution in the samples from Ponti Rossi drilling.

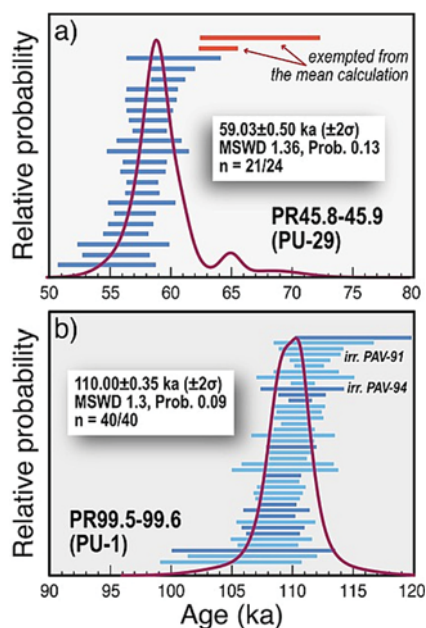


Fig. 9. Cumulative probability and ranked distribution of $^{40}\text{Ar}/^{39}\text{Ar}$ ages of alkali feldspars from selected samples: a) sample PR45.8–45.9 (lowermost sub-unit of PU-29); b) sample 99.5–99.6 (PU-1). Mean age for sample PR99.5–99.6 refers to the pooled weighted mean calculated using data from two irradiations performed at different times (irradiation PAV-91 and PAV-94, see Table S1). Bars are 2σ analytical uncertainties for sample PR45.8–45.9 and 2σ internal uncertainties for sample PR99.5–99.6.

and are considered unreliable. The step-heating run on the individual millimetre-sized grain (Table S1) gave concordant ages for more than 95 % of the total $^{39}\text{Ar}_K$ released, with a weighted mean age of 58.94 ± 0.83 ka, which is in close agreement with the mean age from total fusion data and indicates that alkali feldspars contain negligible to no excess Ar.

Twenty-eight total fusion analyses (Table S1 in Supplementary Material) of the first irradiation of alkali feldspars from sample PR99.50–99.60, collected from the deepest cored unit (PU-1), yielded concordant ages (MSWD 1.18) for all the runs, with a weighted mean age of 110.16 ± 0.43 ka ($\pm 2\sigma$ internal uncertainty). This age is indistinguishable at 1σ level from that calculated from the twelve total fusion analyses of the second irradiation (mean age of 109.67 ± 0.69 ka, MSWD 0.55). Treating the forty total fusion analyses as single samples and using the internal uncertainties on age (Fig. 9b) yields a pooled mean age of 110.00 ± 0.35 ka ($\pm 2\sigma$, MSWD = 1.3).

7. Discussions

7.1. Interpretation of the stratigraphy of the Ponti Rossi borehole

The investigation of the Ponti Rossi borehole (Fig. 4) and the characteristics of the cored sediments (Table 1) permit some preliminary stratigraphic considerations of the past volcanic activity of the Neapolitan Volcanic Area. The cored sediments document not only the occurrence of coarse-grained, thick deposits representing the proximal record of explosive eruptions that occurred in the CF area, but also thinner and finer-grained sediments attributable either to minor explosive eruptions of the continental CF or, alternatively, to medial/distal fall deposits that originated from the insular sector of the CF volcanic district. The presence of paleosols separating the PUs throughout the succession suggests that, over the last 110 ka, sub-aerial conditions persisted in this area, as already reported by Orsi et al. (1996).

Based on the structural and lithological features, as well as on the comparison with the deposits widely exposed in the surroundings, the

shallowest cored unit (PU-31) can be undoubtedly attributed to the ~ 15 ka NYT eruption (Orsi et al., 1992; Scarpati et al., 1993; Cole and Scarpati, 1993; Wohletz et al., 1995), the second largest caldera-forming event of CF, extensively cropping out in the Ponti Rossi area (Orsi et al., 1996) and representing a clear chronostratigraphic marker.

The remaining units (PU-30 and PU-29) of the upper part of the sequence, immediately underlying the NYT (PU-31), are instead not easily relatable to specific eruptions or eruptive sources only based on the stratigraphic characteristics. In the Ponti Rossi area, the surface geological record consists of a stratigraphic succession including at least nine pyroclastic units (PRn to PRv, Pappalardo et al., 1999) sandwiched between the products of NYT and CI eruptions. This interval (15–40 ka) consists of fall deposits, made up of fine to coarse pumice (and very minor scoria) lapilli, and pyroclastic current deposits consisting of massive to planar- to cross-laminated ash layers with scattered to abundant pumice lapilli dispersed. Units range in thickness from a few centimetres to <1 m and are separated by centimetre- to decimetre-thick paleosols or humified layers (Orsi et al., 1996). The CI sequence, whose base is not exposed in the Ponti Rossi area, is mainly composed of lithified, yellow to greyish ash deposits with abundant coarse (up to decimetres in diameter) scoria and pumice clasts and lithic fragments. This deposit represents the zeolitized upper part of the thick welded to sintered ignimbrite sequence found as far as 80 km from CF (e.g., Barberi et al., 1978; Fisher et al., 1993; Scarpati et al., 2020; Silleni et al., 2020, 2024) and emplaced by the most widespread pyroclastic current generated during the CI eruption. The CI sequence has also been recognised in the S51 borehole by Pappalardo et al. (1999, 2002). The authors describe the CI deposits as consisting of four superimposed flow units. Most of the thickness varies upward from a welded, dark grey ash with abundant blackish juvenile clasts to a greyish/pinkish to yellowish sintered ash containing grey pumice and black scoria and abundant lithic lava and hornfelsed clasts. The PU-30 is composed of at least 10 sub-units whose boundaries are marked only by a lithological change and/or structural variations. These characteristics, and above all the lack of any paleosol or even incipient humification of the deposits, rule out a direct correlation with the pyroclastic units, exposed in the Ponti Rossi area, belonging to the 15–40 ka interval. Similarly, the PU-30 shows lithological and structural characteristics that significantly differ from those of the CI deposits (both in exposure and cored in S51 borehole), preventing a certain stratigraphic correlation. The very limited thickness, the fine-grained nature and the emplacement as a fall deposit of some sub-units of PU-30 (Table 1) suggest the possible contribution of eruptions sourced from the insular sector of the Campi Flegrei district besides the continental area. The PU-29 is 16.25 m thick and consists of at least 7 decimetre- to meter-thick sub-units, made up of ash deposits with a variable amount of rounded to sub-rounded pumice lapilli and minor fine ash layers with accretionary lapilli, separated by thin, lithic-rich, colluvial sandy layers. The PU-29 is interpreted as consisting entirely of pyroclastic current deposits emplaced during discrete, magmatic to phreatomagmatic eruptive pulses, separated by the deposition of colluvial sediments. The thin thickness of the colluvial sandy layers and no signs of humification or pedogenesis suggest that the emplacement of PU-29 possibly resulted from very closely spaced eruptions or multiple phases of a single eruption, likely from a nearby source as suggested by the thickness of the deposits. The stratigraphic features of PU-29 and, above all, the radioisotopic age (59.03 ± 0.50 ka) of the lowermost sub-unit of PU-29 provides further evidence that precludes any possible correlation of the whole PU-29 with the CI or younger deposits (~ 15 –40 ka).

The possible absence of the CI deposits would not be surprising when considering the geomorphological aspects of the drilling site. The Ponti Rossi-Capodimonte area is characterized by steep profiles and is incised by subsequent valleys, with a well-developed hydrographic network (Ascione et al., 2021) cutting the pyroclastic sequence down to at least the upper part of the CI sequence. The drilling operations were carried out almost at the outlet of a valley incised along the eastern flank of the

Capodimonte hill. The prolonged stream erosion, which possibly started immediately after the CI eruption and continued during the CI–NYT interval (40–15 ka), may have eroded the whole (or most of the) thickness of the CI deposits and the Ponti Rossi sequence between CI and NYT (units PRn to PRv, dated by Pappalardo et al., 1999 between 16.1 and 15.9 ka). This significant erosional phase coincides with the Last Glacial Maximum characterized by sea lowstand during which the sea level was approximately 120 m lower than present-day (Lambeck and Chappell, 2001; Peltier, 2002). The deep erosion that occurred in the 40–15 ka interval is also confirmed by the remarkable thickness (a minimum of 33 m) of the NYT deposits recovered through a pilot drillhole we performed, in mid-January 2022, a few tens of meters downslope of the main Ponti Rossi drillhole. The pyroclastic currents of the NYT eruption were channelled in this valley and sedimented a thick ash and lapilli deposit. On the other hand, two further hypotheses can be considered as possible explanations: 1) the erosion exerted by the CI pyroclastic currents themselves and/or 2) phases of *syn*-eruptive non-deposition (bypass of the pyroclastic current). As previously reported, in the exposures surrounding our drillhole, as well as in the nearby S51 borehole (Pappalardo et al., 2002), the CI deposits are the proximal counterpart of the thick ignimbrite sequence found throughout the Campanian region (e.g., Fisher et al., 1993; Scarpati et al., 2020; Silleni et al., 2020, 2024) and emplaced by the most energetic pyroclastic current. Scarpati and Perrotta (2012) demonstrated that this pyroclastic current was responsible for a very deep erosion of the underlying fall deposit, with a maximum in the available peri-caldera outcrops and decreasing with the distance from the source. Accordingly, the contribution of the extremely efficient erosive process exerted by the CI pyroclastic current in the Ponti Rossi area caused the Plinian fall deposit and, possibly, part of the thickness of the overlying pyroclastic current deposits to be wiped out. Furthermore, the same pyroclastic current produced a bypass zone (area where the pyroclastic current passes without depositing) around the Campi Flegrei caldera, which resulted in pyroclastic deposits much thinner and with a more chaotic Anisotropy of Magnetic Susceptibility (AMS) fabric than their medial-distal counterparts (Ort et al., 1999, 2003; Scarpati et al., 2020). This reflects the passage of a high-energy and turbulent pyroclastic current with phases of non-deposition associated with strong erosion. However, we assume that the bypass of the pyroclastic current and the *syn*-eruptive erosion are the less relevant processes. Throughout the Ponti Rossi area, the CI deposits crop out with minimum thicknesses up to 10 m (our borehole was emplaced ~20 m from an exposure of the CI deposits whose base is buried, Fig. 3a) and attain a total thickness of 30.1 m in the S51 borehole (Pappalardo et al., 2002). This suggests that the CI deposits would lack only along a narrow strip that coincides with the valley where the drillhole was emplaced. Ultimately, even though all these parameters are not mutually exclusive, the absence (or the presence of a very reduced thickness) of the CI deposits can be mainly the result of the post-depositional, prolonged stream erosion, possibly combined with the minor contribution of the *syn*-eruptive erosion and the bypass of the pyroclastic current. The geochemical characterization of the cored sediments, whose results will be the subject of a future work, will disclose whether a limited thickness of the CI deposits has been preserved.

Regarding the middle part of the sequence, consisting of the 26 PUs, based on structural and textural characteristics (Table 1), most of them (14) are exclusively composed of pyroclastic current deposits while seven PUs (PU-5, PU-6, PU-7, PU-10, PU-11, PU-18 and PU-19) consist of both fall deposits and ash layers emplaced by pyroclastic currents. Only three PUs (PU-3, PU-4 and PU-25) are thin, fine-grained and consist entirely of fall deposits. Two PUs (PU8 and PU26) are interpreted as reworked volcanoclastic units (Table 1) owing to the high lithic content and the lithological heterogeneity and alteration of the juvenile fraction (Fig. 7). More in detail, PU-7 consists of two decimetre-thick fall deposits interbedded with two pyroclastic current deposits. PU-11 consists mainly of decimetre-thick coarse pumice fall layers and minor

pyroclastic current deposits. PU-18 consists of a basal, thin pyroclastic current deposit overlaid by a 0.9 m thick fall deposit. PU-19 is mainly made up of pyroclastic current deposits punctuated by brief fall phases. Due to the relative coarseness of the deposit and the substantial abundance of lithic fragments, it is possible to hypothesise a proximal source. PU-9, PU-12 to PU-17, PU-20 to PU-24, PU-27 and PU-28 are thin pyroclastic current deposits. Apart from some sporadic findings in the topmost samples, samples from PU-12 to PU-19 are featured by the occurrence of leucite or analcime crystals, which could be derived from leucite alteration (Table 1 and Table 2). The occurrence of leucite, both in the juvenile and lithic components, is somewhat anomalous at CF and Ischia whose products are silica saturated and, overall, leucite-free. Samples from these PUs deserve particular attention in future investigations to determinate the reasons for this “anomaly” (vent location, different feeding magmas, etc.).

Finally, about the lower interval, the second deepest and thickest unit (PU-2; 21.5 m) of the sequence appears interesting not only for its decametric thickness but also for the occurrence at ~87 m of depth of oversized lithic fragments possibly emplaced as projectiles (Fig. 5b). These characteristics are diagnostic of a proximal source. PU-2 is completely formed by pyroclastic current deposits, related to both magmatic and phreatomagmatic fragmentation, due to the occurrence of ash deposits with abundant highly vesiculated pumice lapilli and accretionary lapilli-rich layers. This unit could likely represent the flank of a “tuff” cone. In fact, the structure and lithological features are similar to those of the monogenetic tuff cones, older than CI, forming the hilly morphology of the city of Naples and at Monte di Procida (Perrotta et al., 2010; Scarpati et al., 2013, 2015; Santangelo et al., 2024). Alternatively, PU-2 may represent the proximal deposit of an ignimbrite-forming eruption, sourced from the CF area, having a larger areal distribution. The presence of a thin reworked horizon at 75.7 m of depth may suggest a very brief phase of *syn*-eruptive reworking.

Regarding the deepest unit, the remarkable thickness (>17 m), the relative coarseness and the textural characteristics of PU-1 suggest an emplacement from pyroclastic currents from a source located in the continental part of CF volcanic district. The presence of quartz in the PU-1 products, highlighted by the XRD analyses, is linked to the occurrence of lithic fragments from the sedimentary basement (siltite), which could be a diagnostic feature for this pyroclastic units even for proximal-distal correlations.

7.2. Implications for the history of the Neapolitan Volcanic Area explosive activity

The radioisotopic age (59.03 ± 0.50 ka; Fig. 9a) of the lowermost sub-unit of PU-29 (Fig. 4) allows the recognition in the Ponti Rossi borehole of a minimum number of 28 PUs older than the CI, which increases to 29 if we consider the dated sub-unit itself (Fig. 10). Based on the adopted stratigraphic criteria, the 7 sub-units that compose the PU-29 should span a relatively short time interval close to the sub-unit dated at ~59 ka, as the colluvial sands intercalated in PU-29 (Fig. 4 and Table 1) could be either *syn*-eruptive reworking events between very closely spaced eruptive pulses of a single, long-lasting eruption or, in any case, represent short inter-eruptive time intervals. If this is true, the sequence potentially including the pre-CI activity attains a minimum thickness of 79.2 m and represents at least 70 % of the total cored succession (113.2 m). It includes all the PUs belonging to the basal and middle part of the drillhole (plus the PU-29 belonging to the upper part), confirming that the selected site perfectly achieved the main purpose of our research. Even though in our stratigraphic framework each PU does not necessarily correspond to an Eruption Unit (*sensu* Fisher and Schmincke, 1984), at least 29 eruptions older than CI are recognised in the Ponti Rossi borehole. Geochronological, chemical and isotopic investigations are planned to determine the occurrence of multiple Eruptive Units in some single PUs.

The remarkable number of PUs older than 40 ka, never reported in

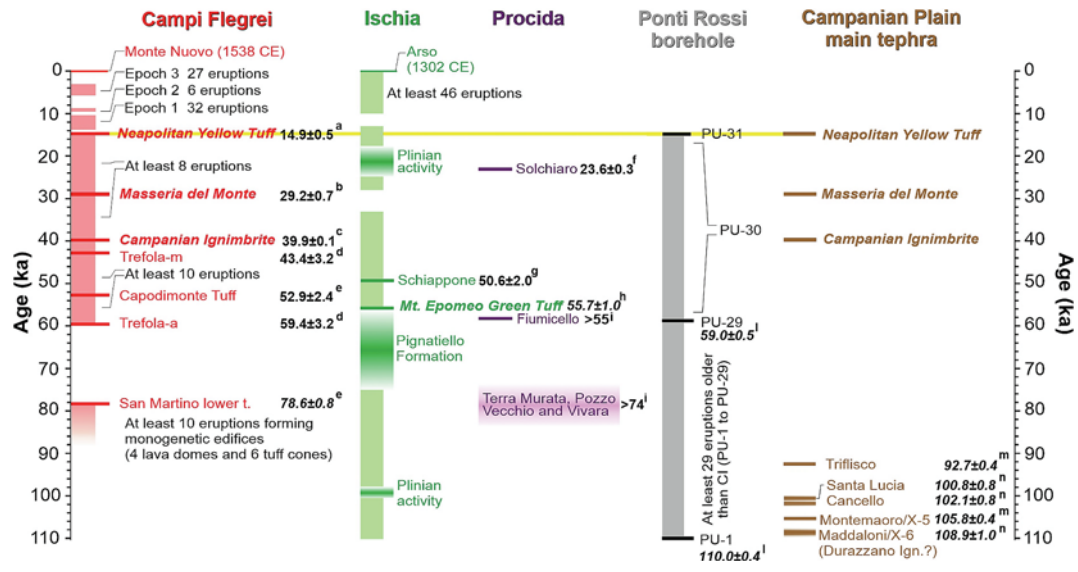


Fig. 10. Summary of the explosive history of Campi Flegrei, Ischia and Procida, as reconstructed from near-vent stratigraphic records, whose products may possibly be represented in the Ponti Rossi borehole. The main mid-distal tephra layers, spanning the ~15–110-ka interval, found in Campanian Plain are also reported. Caldera-forming eruptions are in bold italics. Age (ka) of each tephra is reported in bold. The yellow line indicates the only consistent correlation based on stratigraphic data. Age data source: ^aDeino et al., (2004), ^bAlbert et al., (2019); ^cGiaccio et al., (2017a); ^dPappalardo et al., (1999); ^eScarpati et al., (2013); ^fMorabito et al. (2014); ^gTomlinson et al., (2014); ^hGiaccio et al., (2017b); ⁱPerrotta et al., (2010); ^lthis study; ^mFernandez et al., (2024), ⁿMonaco et al., (2022a). All ages are ⁴⁰Ar/³⁹Ar except for Morabito et al. (2014) and Tomlinson et al. (2014). Literature ⁴⁰Ar/³⁹Ar data are recalculated relative to an ACs age of 1.1848 Ma (Niespolo et al., 2017) adopted in this study. (For interpretation of the references to colour in this figure legend, the reader is referred to the web version of this article.)

any other borehole drilled in nearby areas, and the clear identification of pyroclastic deposits even of minor thickness greatly increase the possibilities for a more detailed reconstruction of the history of the Neapolitan Volcanic Area before the CF caldera formation. In fact, results from our scientific drilling differ from those reported in the S51 borehole where only eleven units underlying the CI, with thicknesses ranging from 0.8 m to 11.7 m, were recognised by Pappalardo et al. (2002). This difference may be attributed to local erosion or reworking/pedogenesis of the thinnest units and to the better quality of the modern drilling techniques. Indeed, the high recovery percentage (~98 %) allowed us to retrieve even very thin units (a few centimetres thick) that may have been lost in the S51 borehole.

The radioisotopic age of the deepest cored unit (PU-1, 110.00±0.35 ka; Fig. 9b) is undoubtedly one of the most relevant results of this study, as it represents the oldest ever age of a volcanic deposit recovered from the CF area, specifically in proximal settings along or close to the caldera rim. The age of PU-1 is significantly older than that obtained on a pyroclastic deposit (San Martino Lower Tephra, ~79 ka; Scarpati et al., 2013) collected at the base of the San Martino hill (Fig. 2), in the city of Naples. It is worth noting that the age of PU-1 is consistent, within uncertainties (2σ level), with that of the Maddaloni tephra (109.3±1.0 ka; 108.9±1.0 ka, recalculated using the same age for the ACs reference material adopted in this study; Fig. 10) collected in medial settings, along the piedmont area of the Apennine reliefs bordering the Campanian Plain, and correlated to the widespread X-6 tephra (Monaco et al., 2022a). The age determination of PU-1 is also indistinguishable from that of the Durazzano Ignimbrite (116.1±4.4 ka, ±1σ; Fig. 2), recognised in the ENE part of the Neapolitan Volcanic Area (Rolandi et al., 2003). While a definitive, robust correlation needs a full geochemical characterization, such a fair chronological consistency suggests that PU-1 could represent the first near-vent evidence that the Maddaloni tephra and its distal equivalent (X-6 tephra), as well as geochemically similar tephra erupted in the same time span, were sourced from the CF area (Fig. 10).

By considering the available geochronological constraints of the shallowest and deepest PUs (~15 ka and ~110 ka, respectively), the borehole recovered a succession representing a 95 ky period of volcanic

activity (Fig. 10), entirely resulting from explosive volcanism. Some units may be the equivalent to the pyroclastic deposits >40 ka recognised in other sectors of the CF caldera (e.g., Pappalardo et al., 1999; Perrotta et al., 2010; Vineberg et al., 2023), in the mid-distal settings (Di Vito et al., 2008; Monaco et al., 2022a), or may be the proximal counterpart of tephra and crypto-tephra reported in the distal marine/terrestrial tephrostratigraphic records (e.g. Tomlinson et al., 2014; Giaccio et al., 2017b; Petrosino et al., 2016; Monaco et al., 2022b; Fernandez et al., 2024). Particularly, the interval 59–110 ka, which brackets the succession from PU-29 to PU-1, may comprise the Campanian Plain MIS 5 tephra layers (Fig. 10) attributed to the CF area and dated between ~92 and ~109 ka (Monaco et al., 2022a). Some units were possibly sourced from the islands of Ischia and Procida, which produced explosive eruptions in the same time interval (Fig. 10).

8. Summary and concluding remarks

The stratigraphic framework of the Ponti Rossi borehole presented in this work is a first step toward future research activities aimed at improving the knowledge of the long-term, late Pleistocene eruptive history of the Neapolitan Volcanic Area, along with its implications on the landscape/environmental evolution. The 113.2 m-long sediment core from the Ponti Rossi area, north of Naples, provided new relevant data on the poorly constrained volcanic activity of the Neapolitan Volcanic Area preceding the CI eruption (~40 ka). The main results are here summarised:

- based on the stratigraphic analysis, thirty-one Pyroclastic Units (PU) were recognised. Not necessarily all of them correspond to Eruptive Units (sensu Fisher and Schmincke, 1984) as specified in the adopted methodology. The shallowest unit (PU-31) is attributed to the 15 ka NYT eruption.
- the ⁴⁰Ar/³⁹Ar data from the deepest cored unit (PU-1) yielded an age of 110.00±0.35 ka, which represents the oldest ever documented activity in the proximal sequences of the CF area; this age is compatible with those of the widespread Mediterranean Maddaloni/X-6 tephra.

- the thirty PUs underlying the NYT, having thicknesses between 0.13 and 21.5 m, are separated by well-developed paleosols or humified reworked materials, suggesting the persistence of sub-aerial environmental conditions in the selected area. Unfortunately, none of the units can be clearly correlated to the CI eruption or eruptions that occurred within the 15–40 ka time interval, making further analysis necessary for reliable attributions and correlations.
- based on the radioisotopic age of the lowermost sub-unit of PU-29 and of the deepest PU-1, a minimum of 29 eruptions are recorded in the time span between ~59 and ~110 ka, whose deposits represent at least 70 % of the retrieved pyroclastic succession.
- the pyroclastic succession between ~59 and ~110 ka consists predominantly of pyroclastic current deposits, resulting from both magmatic and phreatomagmatic fragmentation, and minor fall deposits. Some of these PUs (e.g. PU-1 and PU-2) clearly exhibit features, such as coarseness, lithic enrichment, ballistic clasts and remarkable thickness, compatible with a proximal source.
- At least three units (e.g., PU-3, PU-4 and PU-25) could be products emplaced during low energy eruptions or distal deposits possibly vented from Ischia and Procida.
- Some units (PU-12 to PU-19) are characterized by leucite-bearing juvenile and lithic fragments that appear to be “anomalous” for the volcanism in the CF area.
- Overall, the Ponti Rossi borehole extended the explosive activity preceding the CF caldera formation back to at least 110 ka, adding 30 ka to the previously documented history, and setting the basis for future detailed investigations on this virtually unknown, but relevant, period of the CF volcanic district.

CRediT authorship contribution statement

Domenico Sparice: Writing – review & editing, Writing – original draft, Visualization, Validation, Methodology, Investigation, Formal analysis, Data curation, Conceptualization. **Carlo Pelullo:** Writing – review & editing, Writing – original draft, Visualization, Validation, Methodology, Investigation, Formal analysis, Data curation, Conceptualization. **Sandro de Vita:** Writing – review & editing, Writing – original draft, Visualization, Validation, Supervision, Project administration, Methodology, Investigation, Formal analysis, Data curation, Conceptualization. **Ilenia Arienzo:** Writing – review & editing, Writing – original draft, Visualization, Validation, Methodology, Investigation, Formal analysis, Data curation, Conceptualization. **Paola Petrosino:** Writing – review & editing, Writing – original draft, Visualization, Validation, Methodology, Investigation, Formal analysis, Data curation, Conceptualization. **Angela Mormone:** Writing – review & editing, Writing – original draft, Visualization, Validation, Formal analysis, Data curation. **Gianfranco Di Vincenzo:** Writing – review & editing, Writing – original draft, Visualization, Validation, Formal analysis, Data curation. **Barbara Marfè:** Writing – review & editing, Writing – original draft, Formal analysis. **Bruna Cariddi:** Writing – review & editing, Writing – original draft, Formal analysis. **Maddalena De Lucia:** Writing – review & editing, Writing – original draft. **Enrico Vertech:** Writing – review & editing, Writing – original draft. **Claudia D’Oriano:** Writing – review & editing, Writing – original draft. **Paola Del Carlo:** Writing – review & editing, Writing – original draft. **Alessio Di Roberto:** Writing – review & editing, Writing – original draft. **Biagio Giaccio:** Writing – review & editing, Writing – original draft. **Giovanni Zanchetta:** Writing – review & editing, Writing – original draft. **Mauro Antonio Di Vito:** Writing – review & editing, Writing – original draft, Visualization, Validation, Supervision, Methodology, Investigation, Formal analysis, Data curation, Conceptualization.

Declaration of competing interest

The authors declare the following financial interests/personal relationships which may be considered as potential competing interests:

Sandro de Vita reports financial support was provided by Pianeta Dinamico - Theme 2 TIFEHO. If there are other authors, they declare that they have no known competing financial interests or personal relationships that could have appeared to influence the work reported in this paper.

Data availability

We shared all the data.

Acknowledgements

Financial support was provided by the project TIFEHO (Trachytic Ignimbrites magma-chambers Formation and Evolution in the pre-Holocene history of the Campania volcanic area. Implications on magmatic processes, eruption dynamics, caldera collapse and resurgence), Resp. S. de Vita. The INGV-OV laboratories have been financially supported by the EPOS Research Infrastructure through the contribution of the Italian Ministry of University and Research (MUR). The Ar laser probe facility was realised with the financial support of CNR. We thank S.I.A. srl and Maurizio Cice for logistical mud services. Comments and suggestions provided by Michael Ort and Dario Pedrazzi, and the editorial work by Sonia Calvari, have been very appreciated and contributed to improving the manuscript.

Appendix A. Supplementary data

Supplementary data to this article can be found online at <https://doi.org/10.1016/j.jvolgeores.2024.108209>.

References

- Alberico, I., Petrosino, P., Zeni, G., D’Andrea, F., Lirer, L., 2005. GEOCITY: a drill-hole database as a tool to assess geological hazard in Napoli urban area. *Environ. Geol.* 47 (6), 751–762. <https://doi.org/10.1007/s00254-004-1199-5>.
- Alberico, I., Petrosino, P., Lirer, L., 2011. Volcanic hazard and risk assessment in a multi-source volcanic area: the example of Napoli city (Southern Italy). *Nat. Hazards Earth Syst. Sci.* 11 (4), 1057–1070. <https://doi.org/10.5194/nhess-11-1057-2011>.
- Albert, P.G., Giaccio, B., Isaia, R., Costa, A., Niespolo, E.M., Nomade, S., Pereira, A., Renne, P.R., Hinchliffe, A., Mark, D.F., Brown, R.J., Smith, V.C., 2019. Evidence for a large-magnitude eruption from Campi Flegrei caldera (Italy) at 29 ka. *Geology* 47 (7), 595–599. <https://doi.org/10.1130/g45805.1>.
- Aprile, F., Toccaceli, R.M., 2002. Nuove conoscenze sulla stratigrafia e distribuzione dei depositi ignimbritici quaternari nel sottosuolo della piana del Sarno (Salerno-Campania)-Italia meridionale. *Il Quaternario* 15 (2), 169–174. <https://amq.aiqua.it/index.php/amq/article/view/604>.
- Aprile, F., Sbrana, A., Toccaceli, R.M., 2004. Il ruolo dei depositi piroclastici nell’analisi cronostratigrafica dei terreni quaternari del sottosuolo della Piana Campana (Italia meridionale). *Il Quaternario* 17, 547–554.
- Ascione, A., Aucelli, P.P., Cinque, A., Di Paola, G., Mattei, G., Ruello, M., Ermolli, Russo E., Santangelo, N., Valente, E., 2021. Geomorphology of Naples and the Campi Flegrei: Human and natural landscapes in a restless land. *J. Maps* 17 (4), 18–28. <https://doi.org/10.1080/17445647.2020.1768448>.
- Astori, A., Trasatti, E., Caricchi, L., Polcaro, M., De Martino, P., Acocella, V., Di Vito, M.A., 2024. Tracking the 2007–2023 magma-driven unrest at Campi Flegrei caldera (Italy). *Commun. Earth Environ.* 5 (1), 506.
- Barberi, F., Innocenti, F., Lirer, L., Munno, R., Pescatore, T., Santacroce, R., 1978. The Campanian Ignimbrite: a major prehistoric eruption in the Neapolitan area (Italy). *Bull. Volcanol.* 41 (1), 1–22.
- Barberi, F., Cassano, E., La Torre, P., Sbrana, A., 1991. Structural evolution of Campi Flegrei caldera in light of volcanological and geophysical data. *J. Volcanol. Geotherm. Res.* 48 (1–2), 33–49. <https://doi.org/10.1007/bf02597680>.
- Belkin, H.E., Rolandi, G., Jackson, J.C., Cannatelli, C., Doherty, A.L., Petrosino, P., De Vivo, B., 2016. Mineralogy and geochemistry of the older (> 40 ka) ignimbrites on the Campanian Plain, southern Italy. *J. Volcanol. Geotherm. Res.* 323, 1–18. <https://doi.org/10.1016/j.jvolgeores.2016.05.002>.
- Bellucci, F., Santangelo, N., Santo, A., 2003. Segnalazione di nuovi depositi piroclastici intercalati alle successioni continentali del Pleistocene Superiore-Olocene della porzione nord-orientale della Piana campana. *Alp. Mediterr. Quat.* 16 (2), 279–287.
- Bellucci, F., Milia, A., Rolandi, G., Torrente, M.M., 2006. Structural control on the Upper Pleistocene ignimbrite eruptions in the Neapolitan area (Italy): volcano tectonic faults versus caldera faults. *Develop. Volcanol.* 9, 163–180. [https://doi.org/10.1016/s1871-644x\(06\)80022-7](https://doi.org/10.1016/s1871-644x(06)80022-7).
- Bevilacqua, A., Macedonio, G., Neri, A., Orsi, G., Petrosino, P., 2022a. Volcanic Hazard Assessment at the Campi Flegrei Caldera, Italy. In: *Campi Flegrei: A Restless Caldera*

- in a Densely Populated Area. Springer, Berlin Heidelberg, pp. 311–355. https://doi.org/10.1007/978-3-642-37060-1_12.
- Bevilacqua, A., De Martino, P., Giudicepietro, F., Ricciolino, P., Patra, A., Pitman, E.B., Bursik, M., Voight, B., Flandoli, F., Macedonio, G., Neri, A., 2022b. Data analysis of the unsteadily accelerating GPS and seismic records at Campi Flegrei caldera from 2000 to 2020. *Sci. Rep.* 12 (1), 1–24. <https://doi.org/10.1038/s41598-022-23628-5>.
- Branney, M., Acocella, V., 2015. *Calderas*. In: *The Encyclopedia of Volcanoes*. Academic Press, pp. 299–315. <https://doi.org/10.1016/b978-0-12-385938-9.00016-x>.
- Brocchini, D., Principe, C., Castradori, D., Laurenzi, M.A., Gorla, L., 2001. Quaternary evolution of the southern sector of the Campanian Plain and early Somma-Vesuvius activity: insights from the Trecase 1 well. *Mineral. Petrol.* 73 (1), 67–91. <https://doi.org/10.1007/s007100170011>.
- Brown, R.J., Orsi, G., de Vita, S., 2008. New insights into late Pleistocene explosive volcanic activity and caldera formation on Ischia (southern Italy). *Bull. Volcanol.* 70 (5), 583–603. <https://doi.org/10.1007/s00445-007-0155-0>.
- Brown, R.J., Civetta, L., Arienzo, I., D'Antonio, M., Moretti, R., Orsi, G., Tomlinson, E.L., Albert, P.G., Menzies, M.A., 2014. Geochemical and isotopic insights into the assembly, evolution and disruption of a magmatic plumbing system before and after a cataclysmic caldera-collapse eruption at Ischia volcano (Italy). *Contrib. Mineral. Petrol.* 168 (3), 1–23. <https://doi.org/10.1007/s00410-014-1035-1>.
- Chiodini, G., Caliro, S., Avino, R., Bini, G., Giudicepietro, F., De Cesare, W., Ricciolino, P., Aiuppa, A., Cardellini, C., Petrillo, Z., Selva, J., Siniscalchi, A., Tripaldi, S., 2021. Hydrothermal pressure-temperature control on CO₂ emissions and seismicity at Campi Flegrei (Italy). *J. Volcanol. Geotherm. Res.* 414, 107245. <https://doi.org/10.1016/j.jvolgeores.2021.107245>.
- Cioni, R., Longo, A., Macedonio, G., Santacroce, R., Sbrana, A., Sulpizio, R., Andronico, D., 2003. Assessing pyroclastic fall hazard through field data and numerical simulations: example from Vesuvius. *J. Geophys. Res.* Solid Earth 108 (B2). <https://doi.org/10.1029/2001jb000642>.
- Cole, J.W., Milner, D.M., Spinks, K.D., 2005. Calderas and caldera structures: a review. *Earth Sci. Rev.* 69 (1–2), 1–26. <https://doi.org/10.1016/j.earscirev.2004.06.004>.
- Cole, P.D., Scarpati, C., 1993. A facies interpretation of the eruption and emplacement mechanisms of the upper part of the Neapolitan Yellow Tuff, Campi Flegrei, southern Italy. *Bull. Volcanol.* 55 (5), 311–326. <https://doi.org/10.1007/bf00301143>.
- D'Antonio, M., Arienzo, I., Brown, R.J., Petrosino, P., Pelullo, P., Giaccio, B., 2021. Tephrostratigraphic Marker in Distal Sequences of the Central Mediterranean. *Minerals* 11 (9), 955. <https://doi.org/10.3390/min11090955>.
- D'Antonio, M., Arienzo, I., Di Renzo, V., Civetta, L., Carandente, A., Tonarini, S., 2022. Origin and differentiation history of the magmatic system feeding the Campi Flegrei volcanic field (Italy) constrained by radiogenic and stable isotope data. In: *Campi Flegrei: A Restless Caldera in a Densely Populated Area*. Springer, Berlin Heidelberg, pp. 125–149. https://doi.org/10.1007/978-3-642-37060-1_4.
- De Astis, G., Pappalardo, L., Piochi, M., 2004. Procida volcanic history: new insights into the evolution of the Phlegraean Volcanic District (Campania region, Italy). *Bull. Volcanol.* 66 (7), 622–641. <https://doi.org/10.1007/s00445-004-0345-y>.
- De Martino, P., Dolce, M., Brandi, G., Scarpatò, G., Tammaro, U., 2021. The ground deformation history of the neapolitan volcanic area (Campi Flegrei caldera, Somma-Vesuvius Volcano, and Ischia Island) from 20 years of continuous GPS observations (2000–2019). *Remote Sens.* 13 (14), 2725. <https://doi.org/10.3390/rs13142725>.
- De Natale, G., Troise, C., Mark, D., Mormone, A., Piochi, M., Di Vito, M.A., Isaia, R., Carlino, S., Barra, D., Somma, R., 2016. The Campi Flegrei Deep Drilling Project (CFDDP): New insight on caldera structure, evolution and hazard implications for the Naples area (Southern Italy). *Geochem. Geophys. Geosyst.* 17 (12), 4836–4847. <https://doi.org/10.1002/2015gc006183>.
- De Vivo, B., Rolandi, G., Gans, P.B., Calvert, A., Bohron, W.A., Spera, F.J., Belkin, H.E., 2001. New constraints of pyroclastic eruptive history of the Campanian Volcanic Plain. *Mineral. Petrol.* 73, 47–65. <https://doi.org/10.1007/s007100170010>.
- Deino, A.L., Orsi, G., de Vita, S., Piochi, M., 2004. The age of the Neapolitan Yellow Tuff caldera-forming eruption (Campi Flegrei caldera-Italy) assessed by ⁴⁰Ar/³⁹Ar dating method. *J. Volcanol. Geotherm. Res.* 133 (1–4), 157–170. [https://doi.org/10.1016/s0377-0273\(03\)00396-2](https://doi.org/10.1016/s0377-0273(03)00396-2).
- Del Pezzo, E., Bianco, F., 2024. Space and time distribution of seismic source energy at campi flegrei, Italy through the last unrest phase (1.1. 2000–31.12. 2023). *Phys. Earth Planet. Inter.* 356, 107258.
- Di Girolamo, P., 1970. *Differenziazione gravitativa e curve isochimiche nella "Igneimbrite Campana"*. *Rend. Soc. Ital. Mineral. Petrol.* 26, 3–44.
- Di Renzo, V., Di Vito, M.A., Arienzo, I., Carandente, A., Civetta, L., D'Antonio, M., Giordano, F., Orsi, G., Tonarini, S., 2007. Magmatic history of Somma-Vesuvius on the basis of new geochemical and isotopic data from a deep borehole (Camaldoli della Torre). *J. Petrol.* 48 (4), 753–784. <https://doi.org/10.1093/ptrology/egl081>.
- Di Roberto, A., Smedile, A., Del Carlo, P., De Martini, P.M., Iorio, M., Petrelli, M., Pantosti, D., Pinzi, S., Todrani, A., 2018. Tephra and cryptotephra in a ~ 60,000-year-old lacustrine sequence from the Fucino Basin: new insights into the major explosive events in Italy. *Bull. Volcanol.* 80 (3), 1–23. <https://doi.org/10.1007/s00445-018-1200-x>.
- Di Vincenzo, G., 2022. High precision multi-collector ⁴⁰Ar/³⁹Ar dating of moldavites (central European tektites) reconciles geochronological and paleomagnetic data. *Chem. Geol.* 608, 121026. <https://doi.org/10.1016/j.chemgeo.2022.121026>.
- Di Vincenzo, G., Folco, L., Suttle, M.D., Brase, L., Harvey, R.P., 2021. Multi-collector ⁴⁰Ar/³⁹Ar dating of microtektites from Transantarctic Mountains (Antarctica): a definitive link with the Australasian tektite/microtektite strewn field. *Geochim. Cosmochim. Acta* 298, 112–130. <https://doi.org/10.1016/j.gca.2021.01.046>.
- Di Vito, M.A., Lirer, L., Mastrolorenzo, G., Rolandi, G., 1987. The 1538 Monte Nuovo eruption (Campi Flegrei, Italy). *Bull. Volcanol.* 49 (4), 608–615. <https://doi.org/10.1007/bf01079966>.
- Di Vito, M.A., Isaia, R., Orsi, G., Southon, J.D., De Vita, S., D'Antonio, M., Pappalardo, L., Piochi, M., 1999. Volcanism and deformation since 12,000 years at the Campi Flegrei caldera (Italy). *J. Volcanol. Geotherm. Res.* 91 (2–4), 221–246. [https://doi.org/10.1016/s0377-0273\(99\)00037-2](https://doi.org/10.1016/s0377-0273(99)00037-2).
- Di Vito, M.A., Sulpizio, R., Zanchetta, G., D'Orazio, M., 2008. The late Pleistocene pyroclastic deposits of the Campanian Plain: new insights into the explosive activity of Neapolitan volcanoes. *J. Volcanol. Geotherm. Res.* 177 (1), 19–48. <https://doi.org/10.1016/j.jvolgeores.2007.11.019>.
- Di Vito, M.A., Acocella, V., Aiello, G., Barra, D., Battaglia, M., Carandente, A., Del Gaudio, C., de Vita, S., Ricciardi, G.P., Ricco, C., Scandone, R., Terrasi, F., 2016. Magma transfer at Campi Flegrei caldera (Italy) before the 1538 AD eruption. *Sci. Rep.* 6 (1), 1–9. <https://doi.org/10.1038/srep32245>.
- D'Oriano, C., Poggianti, E., Bertagnini, A., Cioni, R., Landi, P., Polacci, M., Rosi, M., 2005. Changes in eruptive style during the AD 1538 Monte Nuovo eruption (Phlegraean Fields, Italy): the role of syn-eruptive crystallization. *Bull. Volcanol.* 67, 601–621. <https://doi.org/10.1007/s00445-004-0397-z>.
- Fedele, L., Morra, V., Perrotta, A., Scarpati, C., 2006. *Volcanological and geochemical features of the products of the Fiumicello eruption, Procida island, Campi Flegrei (southern Italy)*. *Period. Mineral.* 75 (1), 43–72.
- Fedele, L., Scarpati, C., Lanphere, M., Melluso, L., Morra, V., Perrotta, A., Ricci, G., 2008. The Breccia Museo formation, Campi Flegrei, southern Italy: geochronology, chemostratigraphy and relationship with the Campanian Ignimbrite eruption. *Bull. Volcanol.* 70, 1189–1219. <https://doi.org/10.1007/s00445-008-0197-y>.
- Fedele, L., Scarpati, C., Sparice, D., Perrotta, A., Laiena, F., 2016. A chemostratigraphic study of the Campanian Ignimbrite eruption (Campi Flegrei, Italy): insights on magma chamber withdrawal and deposit accumulation as revealed by compositionally zoned stratigraphic and facies framework. *J. Volcanol. Geotherm. Res.* 324, 105–117. <https://doi.org/10.1016/j.jvolgeores.2016.05.019>.
- Fernandez, G., Giaccio, B., Costa, A., Monaco, L., Nomade, S., Albert, P.G., Pereira, A., Flynn, M., Leicher, N., Lucchi, F., Petrosino, P., Palladino, D.M., Milia, A., Insinga, D., Wulf, S., Kearney, R., Veres, D., Jordanova, D., Putignano, M.L., Isaia, R., Sottili, G., 2024. New constraints on the Middle-late Pleistocene Campi Flegrei explosive activity and Mediterranean tephrostratigraphy (~ 160 ka and 110–90 ka). *Quat. Sci. Rev.* 331, 108623. <https://doi.org/10.1016/j.quascirev.2024.108623>.
- Fisher, R.V., Schmincke, H.-U., 1984. *Pyroclastic Rocks*. Springer Verlag, Berlin, p. 472.
- Fisher, R.V., Orsi, G., Ort, M., Heiken, G., 1993. Mobility of a large-volume pyroclastic flow—emplacement of the Campanian Ignimbrite, Italy. *J. Volcanol. Geotherm. Res.* 56 (3), 205–220. [https://doi.org/10.1016/0377-0273\(93\)90017-1](https://doi.org/10.1016/0377-0273(93)90017-1).
- Geyer, A., Martí, J., 2009. Stress fields controlling the formation of nested and overlapping calderas: implications for the understanding of caldera unrest. *J. Volcanol. Geotherm. Res.* 181 (3–4), 185–195. <https://doi.org/10.1016/j.jvolgeores.2009.01.018>.
- Giaccio, B., Nomade, S., Wulf, S., Isaia, R., Sottili, G., Cavuoto, G., Galli, P., Messina, P., Spostato, A., Sulpizio, R., Zanchetta, G., 2012. The late MIS 5 Mediterranean tephra markers: a reappraisal from peninsular Italy terrestrial records. *Quat. Sci. Rev.* 56, 31–45. <https://doi.org/10.1016/j.quascirev.2012.09.009>.
- Giaccio, B., Hajdas, I., Isaia, R., Deino, A., Nomade, S., 2017a. High-precision ¹⁴C and ⁴⁰Ar/³⁹Ar dating of the Campanian Ignimbrite (Y-5) reconciles the time-scales of climatic-cultural processes at 40 ka. *Sci. Rep.* 7 (1), 1–10. <https://doi.org/10.1038/srep45940>.
- Giaccio, B., Niespolo, E.M., Pereira, A., Nomade, S., Renne, P.R., Albert, P.G., Arienzo, I., Regattieri, E., Wagner, B., Zanchetta, G., Gaeta, M., Galli, P., Mannella, G., Peronace, E., Sottili, G., Florindo, F., Leicher, N., Marra, F., Tomlinson, E.L., 2017b. First integrated tephrochronological record for the last ~ 190 kyr from the Fucino Quaternary lacustrine succession, Central Italy. *Quat. Sci. Rev.* 158, 211–234. <https://doi.org/10.1016/j.quascirev.2017.01.004>.
- Giacomuzzi, G., Chiarabba, C., Bianco, F., De Gori, P., Agostinetti, N.P., 2024. Tracking transient changes in the plumbing system at Campi Flegrei Caldera. *Earth Planet. Sci. Lett.* 637, 118744. <https://doi.org/10.5194/egusphere-2024-7629>.
- Goody, R.J., Brown, D.J., Goodenough, K.M., Kerr, A.C., 2018. A proximal record of caldera-forming eruptions: the stratigraphy, eruptive history and collapse of the Palaeogene Arran caldera, western Scotland. *Bull. Volcanol.* 80 (9), 1–22. <https://doi.org/10.1007/s00445-018-1243-z>.
- Insinga, D.D., Tamburrino, S., Lirer, F., Vezzoli, L., Barra, M., De Lange, G.J., Tiepolo, M., Vallefuoco, M., Mazzola, S., Sprovieri, M., 2014. Tephrochronology of the astronomically-tuned KC01B deep-sea core, Ionian Sea: insights into the explosive activity of the Central Mediterranean area during the last 200 ka. *Quat. Sci. Rev.* 85, 63–84. <https://doi.org/10.1016/j.quascirev.2013.11.019>.
- Isaia, R., D'Antonio, M., Dell'Erba, F., Di Vito, M., Orsi, G., 2004. *The Astroni volcano: the only example of closely spaced eruptions in the same vent area during the recent history of the Campi Flegrei caldera (Italy)*. *J. Volcanol. Geotherm. Res.* 133 (1–4), 171–192.
- Isaia, R., Vitale, S., Marturano, A., Aiello, G., Barra, D., Ciarcia, S., Iannuzzi, E., Tramparulo, F.D.A., 2019. High-resolution geological investigations to reconstruct the long-term ground movements in the last 15 kyr at Campi Flegrei caldera (southern Italy). *J. Volcanol. Geotherm. Res.* 385, 143–158. <https://doi.org/10.1016/j.jvolgeores.2019.07.012>.
- Isaia, R., Di Giuseppe, M.G., Natale, J., Tramparulo, F.D.A., Troiano, A., Vitale, S., 2021. Volcano-tectonic setting of the Pisciarelli fumarole field, Campi Flegrei caldera, southern Italy: insights into fluid circulation patterns and hazard scenarios. *Tectonics* 40 (5), e2020TC006227. <https://doi.org/10.1029/2020tc006227>.
- Lambeck, K., Chappell, J., 2001. Sea level change through the last glacial cycle. *Science* 292 (5517), 679–686. <https://doi.org/10.1126/science.1059549>.
- Lee, J.-Y., Marti, K., Severinghaus, J.P., Kawamura, K., Yoo, H.-S., Lee, J.B., Kim, J.S., 2006. A redetermination of the isotopic abundances of atmospheric Ar. *Geochim.*

- Cosmochim. Acta 70 (17), 4507–4512. <https://doi.org/10.1016/j.gca.2006.06.1563>.
- Lirer, L., Luongo, G., Scandone, R., 1987. On the volcanological evolution of Campi Flegrei. EOS Trans. Am. Geophys. Union 68 (16), 226–234. <https://doi.org/10.1029/eo068i016p00226>.
- Lirer, L., Petrosino, P., Alberico, I., 2010. Hazard and risk assessment in a complex multi-source volcanic area: the example of the Campania Region, Italy. Bull. Volcanol. 72, 411–429. <https://doi.org/10.1007/s00445-009-0334-2>.
- Lucchi, F., 2013. Stratigraphic methodology for the geological mapping of volcanic areas: insights from the Aeolian archipelago (southern Italy). Geol. Soc. Lond. Mem. 37, 37e53. <https://doi.org/10.1144/m37.5>.
- Lucchi, F., Tranne, C.A., Rossi, P.L., 2010. Stratigraphic approach to geological mapping of the late-Quaternary volcanic island of Lipari (Aeolian archipelago, Southern Italy). Stratigraphy and Geology of Volcanic areas. Geol. Soc. Am. Bull. Special Papers 464, 1–32. [https://doi.org/10.1130/2010.2464\(01\)](https://doi.org/10.1130/2010.2464(01)).
- Maggiore, L., 1934. Information on volcanic materials of Campania used in building construction. Estr. Rel. Serv. Min. Statistiche Ind. Estr. 45 (60), 57–61.
- Marianelli, P., Sbrana, A., Proto, M., 2006. Magma chamber of the Campi Flegrei supervolcano at the time of eruption of the Campanian Ignimbrite. Geology 34 (11), 937–940. <https://doi.org/10.1130/g22807a.1>.
- Martí, J., Gropelli, G., da Silveira, A.B., 2018. Volcanic stratigraphy: a review. J. Volcanol. Geotherm. Res. 357, 68–91.
- Matthews, I.P., Trincardi, F., Lowe, J.J., Bourne, A.J., MacLeod, A., Abbott, P.M., Andersen, N., Asioni, A., Blockley, S.P.E., Lane, C.S., Oh, Y.A., Satow, C.S., Staff, R.A., Wulf, S., 2015. Developing a robust tephrochronological framework for late Quaternary marine records in the Southern Adriatic Sea: new data from core station SA03-11. Quat. Sci. Rev. 118, 84–104. <https://doi.org/10.1016/j.quascirev.2014.10.009>.
- Melluso, L., Morra, V., Perrotta, A., Scarpati, C., Adabbo, M., 1995. The eruption of the Breccia Museo (Campi Flegrei, Italy): fractional crystallization processes in a shallow, zoned magma chamber and implications for the eruptive dynamics. J. Volcanol. Geotherm. Res. 68 (4), 325–339. [https://doi.org/10.1016/0377-0273\(95\)00020-5](https://doi.org/10.1016/0377-0273(95)00020-5).
- Milia, A., Torrente, M.M., 2020. Space-time evolution of an active volcanic field in an extensional region: the example of the Campania margin (eastern Tyrrhenian Sea). Int. J. Vesuvius, Campi Flegrei, and Campanian Volcanism. Elsevier, pp. 297–321. <https://doi.org/10.1016/b978-0-12-816454-9.00012-2>.
- Min, K., Mundil, R., Renne, P.R., Ludwig, K.R., 2000. A test for systematic errors in $^{40}\text{Ar}/^{39}\text{Ar}$ geochronology through comparison with U–Pb analysis of a 1.1 Ga rhyolite. Geochim. Cosmochim. Acta 64, 73–98. [https://doi.org/10.1016/S0016-7037\(99\)00204-5](https://doi.org/10.1016/S0016-7037(99)00204-5).
- Monaco, L., Palladino, D.M., Albert, P.G., Arienzo, I., Conticelli, S., Di Vito, M., Frabrizio, A., D'Antonio, M., Isaia, R., Manning, C.J., Nomade, S., Pereira, A., Petrosino, P., Sottili, G., Sulpizio, R., Zanchetta, G., Giaccio, B., 2022a. Linking the Mediterranean MIS 5 tephra markers to Campi Flegrei (southern Italy) 109–92 ka explosive activity and refining the chronology of MIS 5c-d millennial-scale climate variability. Glob. Planet. Chang. 211, 103785. <https://doi.org/10.1016/j.gloplacha.2022.103785>.
- Monaco, L., Leicher, N., Palladino, D.M., Arienzo, I., Marra, F., Petrelli, M., Nomade, S., Pereira, A., Sottili, G., Conticelli, S., D'Antonio, M., Frabrizio, A., Jicha, B.R., Mannella, G., Petrosino, P., Regattieri, E., Polychronis, C.T., Wagner, B., Zanchetta, G., Giaccio, B., 2022b. The Fucino 250–170 ka tephra record: New insights on peri-Tyrrhenian explosive volcanism, central mediterranean tephrochronology, and timing of the MIS 8-6 climate variability. Quat. Sci. Rev. 296, 107797. <https://doi.org/10.1016/j.quascirev.2022.107797>.
- Morabito, S., Petrosino, P., Milia, A., Sprovieri, M., Tamburrino, S., 2014. A multidisciplinary approach for reconstructing the stratigraphic framework of the last 40 ka in a bathyal area of the eastern Tyrrhenian Sea. Glob. Planet. Chang. 123, 121–138. <https://doi.org/10.1016/j.gloplacha.2014.10.005>.
- Natale, J., Camanni, G., Ferranti, L., Isaia, R., Sacchi, M., Spiess, V., Steinmann, L., Vitale, S., 2022a. Fault systems in the offshore sector of the Campi Flegrei caldera (southern Italy): Implications for nested caldera structure, resurgent dome, and volcano-tectonic evolution. J. Struct. Geol. 163, 104723. <https://doi.org/10.1016/j.jsg.2022.104723>.
- Natale, J., Ferranti, L., Isaia, R., Marino, C., Sacchi, M., Spiess, V., Steinmann, L., Vitale, S., 2022b. Integrated on-land-offshore stratigraphy of the Campi Flegrei caldera: New insights into the volcano-tectonic evolution in the last 15 kyr. Basin Res. 34 (2), 855–882. <https://doi.org/10.1111/bre.12643>.
- Németh, K., Palmer, J., 2019. Geological mapping of volcanic terrains: Discussion on concepts, facies models, scales, and resolutions from New Zealand perspective. J. Volcanol. Geotherm. Res. 385, 27–45. <https://doi.org/10.1016/j.jvolgeores.2018.11.028>.
- Niespolo, E.M., Rutte, D., Deino, A.L., Renne, P.R., 2017. Intercalibration and age of the Alder Creek sanidine $40\text{Ar}/^{39}\text{Ar}$ standard. Quat. Geochronol. 39, 205–213. <https://doi.org/10.1016/j.quageo.2016.09.004>.
- Orsi, G., 2022. Volcanic and Deformation history of the Campi Flegrei Volcanic Field, Italy. Campi Flegrei 1-53. https://doi.org/10.1007/978-3-642-37060-1_1.
- Orsi, G., D'Antonio, M., de Vita, S., Gallo, G., 1992. The Neapolitan Yellow Tuff, a large-magnitude trachytic phreatoplinian eruption: eruptive dynamics, magma withdrawal and caldera collapse. J. Volcanol. Geotherm. Res. 53 (1–4), 275–287. [https://doi.org/10.1016/0377-0273\(92\)90086-s](https://doi.org/10.1016/0377-0273(92)90086-s).
- Orsi, G., De Vita, S., Di Vito, M., 1996. The restless, resurgent Campi Flegrei nested caldera (Italy): constraints on its evolution and configuration. J. Volcanol. Geotherm. Res. 74 (3–4), 179–214. [https://doi.org/10.1016/s0377-0273\(96\)00063-7](https://doi.org/10.1016/s0377-0273(96)00063-7).
- Orsi, G., Di Vito, M.A., Isaia, R., 2004. Volcanic hazard assessment at the restless Campi Flegrei caldera. Bull. Volcanol. 66 (6), 514–530. https://doi.org/10.1007/978-3-642-37060-1_12.
- Orsi, G., Di Vito, M.A., Selva, J., Marzocchi, W., 2009. Long-term forecast of eruption style and size at Campi Flegrei caldera (Italy). Earth Planet. Sci. Lett. 287 (1–2), 265–276. <https://doi.org/10.1016/j.epsl.2009.08.013>.
- Ort, M.H., Rosi, M., Anderson, C.D., 1999. Correlation of deposits and vent locations of the proximal Campanian Ignimbrite deposits, Campi Flegrei, Italy, based on natural remanent magnetization and anisotropy of magnetic susceptibility characteristics. J. Volcanol. Geotherm. Res. 91 (2–4), 167–178.
- Ort, M.H., Orsi, G., Pappalardo, L., Fisher, R.V., 2003. Anisotropy of magnetic susceptibility studies of depositional processes in the Campanian Ignimbrite, Italy. Bull. Volcanol. 65, 55–72.
- Pabst, S., Wörner, G., Civetta, L., Tesoro, R., 2008. Magma chamber evolution prior to the Campanian ignimbrite and Neapolitan Yellow Tuff eruptions (Campi Flegrei, Italy). Bull. Volcanol. 70, 961–976. <https://doi.org/10.1007/s00445-007-0180-z>.
- Pappalardo, L., Civetta, L., d'Antonio, M., Deino, A., Di Vito, M., Orsi, G., Carandente, A., de Vita, S., Isaia, R., Piochi, M., 1999. Chemical and Sr-isotopic evolution of the Phlegraean magmatic system before the Campanian Ignimbrite and the Neapolitan Yellow Tuff eruptions. J. Volcanol. Geotherm. Res. 91 (2–4), 141–166. [https://doi.org/10.1016/s0377-0273\(99\)00033-5](https://doi.org/10.1016/s0377-0273(99)00033-5).
- Pappalardo, L., Civetta, L., De Vita, S., Di Vito, M., Orsi, G., Carandente, A., Fisher, R.V., 2002. Timing of magma extraction during the Campanian Ignimbrite eruption (Campi Flegrei Caldera). J. Volcanol. Geotherm. Res. 114 (3–4), 479–497. [https://doi.org/10.1016/s0377-0273\(01\)00302-x](https://doi.org/10.1016/s0377-0273(01)00302-x).
- Peltier, W.R., 2002. On eustatic sea level history: last Glacial Maximum to Holocene. Quat. Sci. Rev. 21 (1–3), 377–396. [https://doi.org/10.1016/s0277-3791\(01\)00084-1](https://doi.org/10.1016/s0277-3791(01)00084-1).
- Pelullo, C., Arienzo, I., D'Antonio, M., Giaccio, B., Iovine, R.S., Leicher, N., Palladino, D. M., Petrelli, M., Petrosino, P., Russo, Ermolli E., Sottili, G., Totaro, F., Zanchetta, G., 2024. Explosive volcanic activity in Central-Southern Italy during Middle Pleistocene: a tale from tephra layers of the Acerno basin. Quat. Sci. Adv. 14, 100186. <https://doi.org/10.1016/j.qsa.2024.100186>.
- Pennetta, M., Russo, F., Donadio, C., 2014. Late Quaternary environmental evolution of the intermontane Valle Caudina basin, southern Italy. Rendic. Lincei 25 (2), 231–240. <https://doi.org/10.1007/s12210-014-0334-9>.
- Perrotta, A., Scarpati, C., 1994. The dynamics of the Breccia Museo eruption (Campi Flegrei, Italy) and the significance of spatter clasts associated with lithic breccias. J. Volcanol. Geotherm. Res. 59 (4), 335–355. [https://doi.org/10.1016/0377-0273\(94\)90086-8](https://doi.org/10.1016/0377-0273(94)90086-8).
- Perrotta, A., Scarpati, C., Luongo, G., Morra, V., 2006. The Campi Flegrei caldera boundary in the city of Naples. Volcanism in the Campania Plain - Vesuvius. Campi Flegrei Ignimbri. 9, 85–96. [https://doi.org/10.1016/s1871-644x\(06\)80019-7](https://doi.org/10.1016/s1871-644x(06)80019-7).
- Perrotta, A., Scarpati, C., Luongo, G., Morra, V., 2010. Stratigraphy and volcanological evolution of the southwestern sector of Campi Flegrei and Procida Island, Italy. Stratigraphy and geology of volcanic areas. Geol. Soc. Am. 171–191. [https://doi.org/10.1130/2010.2464\(09\)](https://doi.org/10.1130/2010.2464(09)) (Special Paper, 464).
- Petrosino, P., Morabito, S., Jicha, B.R., Milia, A., Sprovieri, M., Tamburrino, S., 2016. Multidisciplinary tephrochronological correlation of marker vents in the eastern Tyrrhenian Sea between 48 and 105 ka. J. Volcanol. Geotherm. Res. 315, 79–99. <https://doi.org/10.1016/j.jvolgeores.2021.107461>.
- Petrosino, P., Arienzo, I., Mazzeo, F.C., Natale, J., Petrelli, M., Milia, A., Perugini, D., D'Antonio, M., 2019. The San Gregorio Magno lacustrine basin (Campania, southern Italy): improved characterization of the tephrostratigraphic markers based on trace elements and isotopic data. J. Quat. Sci. 34 (6), 393–404. <https://doi.org/10.1002/jqs.3107>.
- Petrosino, P., Angrisani, A.C., Barra, D., Donadio, C., Aiello, G., Allocca, V., Coda, S., De Vita, P., Jicha, B.R., Calcaterra, D., 2021. Multiproxy approach to urban geology of the historical center of Naples, Italy. Quat. Int. 577, 147–165. <https://doi.org/10.1016/j.quaint.2020.12.043>.
- Piochi, M., Mastrolorenzo, G., Pappalardo, L., 2005. Magma ascent and eruptive processes from textural and compositional features of Monte Nuovo pyroclastic products, Campi Flegrei, Italy. Bull. Volcanol. 67, 663–678. <https://doi.org/10.1007/s00445-005-0410-1>.
- Piochi, M., Kilburn, C.R.J., Di Vito, M.A., Mormone, A., Tramelli, A., Troise, C., De Natale, G., 2014. The volcanic and geothermally active Campi Flegrei caldera: an integrated multidisciplinary image of its buried structure. Int. J. Earth Sci. 103, 401–421. <https://doi.org/10.1007/s00531-013-0972-7>.
- Pistolesi, M., Isaia, R., Marianelli, P., Bertagnini, A., Fourmentaux, C., Albert, P.G., Tomlison, E.L., Menzies, M.A., Rosi, M., Sbrana, A., 2016. Simultaneous eruptions from multiple vents at Campi Flegrei (Italy) highlight new eruption processes at calderas. Geology 44 (6), 487–490. <https://doi.org/10.1130/g37870.1>.
- Rittmann, A., 1950. Geological survey of Camaldoli Hill in Campi Flegrei. Boll. Soc. Geol. It. 49, 48 (in Italian).
- Rolandi, G., Bellucci, F., Heizler, M.T., Belkin, H.E., De Vivo, B., 2003. Tectonic controls on the genesis of ignimbrites from the Campanian Volcanic Zone, southern Italy. Mineral. Petrol. 79 (1), 3–31. <https://doi.org/10.1007/s00710-003-0014-4>.
- Rolandi, G., De Natale, G., Kilburn, C.R., Troise, C., Somma, R., Di Lascio, M., Fedele, A., Rolandi, R., 2020. The 39 ka Campanian Ignimbrite eruption: New data on source area in the Campanian Plain. In: Vesuvius, Campi Flegrei, and Campanian Volcanism. Elsevier, pp. 175–205. <https://doi.org/10.1016/b978-0-12-816454-9.00008-0>.
- Romano, P., Santo, A., Voltaggio, M., 1994. L'evoluzione geo-morfologica della Pianura del Fiume Volturno (Campania) durante il tardo Quaternario (Pleistocene medio superiore-Olocene). Il Quaternario 7 (1), 41–56.

- Romano, P., Di Vito, M.A., Giampaola, D., Cinque, A., Bartoli, C., Boenzi, G., Detta, F., Di Marco, M., Giglio, M., Iodice, S., Liuzza, V., Ruello, M.R., di Cola, C.S., 2013. Intersection of exogenous, endogenous and anthropogenic factors in the Holocene landscape: a study of the Naples coastline during the last 6000 years. *Quat. Int.* 303, 107–119. <https://doi.org/10.1016/j.quaint.2013.03.031>.
- Rosi, M., Sbrana, A., 1987. Phlegrean fields. *Quader. Ricerca Scient.* 9 (114).
- Rosi, M., Sbrana, A., Principe, C., 1983. The Phlegrean Fields: structural evolution, volcanic history and eruptive mechanisms. *J. Volcanol. Geotherm. Res.* 17 (1–4), 273–288. [https://doi.org/10.1016/0377-0273\(83\)90072-0](https://doi.org/10.1016/0377-0273(83)90072-0).
- Rosi, M., Sbrana, A., Vezzoli, L., 1988. Correlazioni tefrostratigrafiche di alcuni livelli di Ischia, Procida e Campi Flegrei. *Mem. Soc. Geol. Ital.* 41, 1015–1027.
- Rosi, M., Vezzoli, L., Castelmennano, A., Grieco, G., 1999. Plinian pumice fall deposit of the Campanian Ignimbrite eruption (Phlegrean Fields, Italy). *J. Volcanol. Geotherm. Res.* 91 (2–4), 179–198. [https://doi.org/10.1016/s0377-0273\(99\)00035-9](https://doi.org/10.1016/s0377-0273(99)00035-9).
- Sacchi, M., De Natale, G., Spiess, V., Steinmann, L., Acocella, V., Corradino, M., de Silva, S., Fedele, A., Fedele, L., Geshi, N., Kilburn, C., Insinga, D., Jurado, M.J., Molisso, F., Petrosino, P., Passaro, S., Pepe, F., Porfido, S., Scarpati, C., Schmincke, H.U., Somma, R., Sumita, M., Tamburrino, S., Troise, C., Vallefucio, M., Ventura, G., 2019. A roadmap for amphibious drilling at the Campi Flegrei caldera: Insights from a MagellanPlus workshop. *Sci. Drill.* 26, 29–46. <https://doi.org/10.5194/sd-26-29-2019>.
- Santangelo, I., Scarpati, C., Perrotta, A., Fedele, L., Cole, P., Cioni, R., D’Orlando, C., De Micheli Vitturi, M., Pardini, F., Speranza, F., 2024. Unveiling the Ancient History of the Southwestern Sector of Campi Flegrei through the stratigraphy compositional Variability and Physical Volcanology of the Pre-caldera VitaFumo and Miliscola Tuff Cones. *Miscellanea INGV* 83, 63. 6th Conference A. Rittmann, 18–20 September 2024, Catania, Italy.
- Santangelo, N., Romano, P., Ascione, A., Ermolli, E.R., 2017. Quaternary evolution of the Southern Apennines coastal plains: a review. *Geol. Carpath.* 68 (1), 43. <https://doi.org/10.1515/geoca-2017-0004>.
- Sbrana, A., Marianelli, P., Pasquini, G., 2018. Volcanology of Ischia (Italy). *J. Maps* 14 (2), 494–503. <https://doi.org/10.1080/17445647.2018.1498811>.
- Sbrana, A., Marianelli, P., Pasquini, G., 2021. The Phlegrean Fields volcanological evolution. *J. Maps* 17 (2), 557–570. <https://doi.org/10.1080/17445647.2021.1982033>.
- Scandone, R., Bellucci, F., Lirer, L., Rolandi, G., 1991. The structure of the Campanian Plain and the activity of the Neapolitan volcanoes (Italy). *J. Volcanol. Geotherm. Res.* 48 (1–2), 1–31. [https://doi.org/10.1016/0377-0273\(91\)90030-4](https://doi.org/10.1016/0377-0273(91)90030-4).
- Scarpa, R., Bianco, F., Capuano, P., Castellano, M., D’Auria, L., Lieto, B.D., Romano, P., 2022. Historic Unrest of the Campi Flegrei Caldera, Italy. In: *Campi Flegrei*. Springer, Berlin, Heidelberg, pp. 257–282. https://doi.org/10.1007/978-3-642-37060-1_10.
- Scarpati, C., Perrotta, A., 2012. Erosional characteristics and behaviour of large pyroclastic density currents. *Geology* 40 (11), 1035–1038.
- Scarpati, C., Perrotta, A., 2016. Stratigraphy and physical parameters of the Plinian phase of the Campanian Ignimbrite eruption. *GSA Bull.* 128 (7–8), 1147–1159. <https://doi.org/10.1130/b31331.1>.
- Scarpati, C., Cole, P., Perrotta, A., 1993. The Neapolitan Yellow Tuff—a large volume multiphase eruption from Campi Flegrei, southern Italy. *Bull. Volcanol.* 55 (5), 343–356. <https://doi.org/10.1007/bf00301145>.
- Scarpati, C., Perrotta, A., Lepore, S., Calvert, A., 2013. Eruptive history of Neapolitan volcanoes: constraints from 40Ar–39Ar dating. *Geol. Mag.* 150 (3), 412–425. <https://doi.org/10.1017/s0016756812000854>.
- Scarpati, C., Sparice, D., Perrotta, A., 2014. A crystal concentration method for calculating ignimbrite volume from distal ash-fall deposits and a reappraisal of the magnitude of the Campanian Ignimbrite. *J. Volcanol. Geotherm. Res.* 280, 67–75. <https://doi.org/10.1016/j.jvolgeores.2014.05.009>.
- Scarpati, C., Perrotta, A., Sparice, D., 2015. Volcanism in the city of Naples. *Rend. Online Soc. Geol. Ital.* 33. <https://doi.org/10.3301/rol.2015.21>.
- Scarpati, C., Sparice, D., Perrotta, A., 2016. Comparative proximal features of the main Plinian deposits (Campanian Ignimbrite and Pomici di Base) of Campi Flegrei and Vesuvius. *J. Volcanol. Geotherm. Res.* 321, 149–157. <https://doi.org/10.1016/j.jvolgeores.2016.04.040>.
- Scarpati, C., Sparice, D., Perrotta, A., 2020. Dynamics of large pyroclastic currents inferred by the internal architecture of the Campanian Ignimbrite. *Sci. Rep.* 10 (1), 1–13. <https://doi.org/10.1038/s41598-020-79164-7>.
- Silleni, A., Giordano, G., Isaia, R., Ort, M.H., 2020. The magnitude of the 39.8 ka Campanian Ignimbrite eruption, Italy: method, uncertainties and errors. *Front. Earth Sci.* 8, 543399. <https://doi.org/10.3389/feart.2020.543399>.
- Silleni, A., Giordano, G., Ort, M.H., Isaia, R., 2024. Transport and deposition of the 39.8 ka Campanian Ignimbrite large-scale pyroclastic density currents (Italy). *Geol. Soc. Am. Bull.* <https://doi.org/10.1130/B37500.1>.
- Smith, V.C., Isaia, R., Pearce, N.J.G., 2011. Tephrostratigraphy and glass compositions of post-15 kyr Campi Flegrei eruptions: implications for eruption history and chronostratigraphic markers. *Quat. Sci. Rev.* 30 (25–26), 3638–3660. <https://doi.org/10.1016/j.quascirev.2011.07.012>.
- Steinmann, L., Spiess, V., Sacchi, M., 2016. The Campi Flegrei caldera (Italy): formation and evolution in interplay with sea-level variations since the Campanian Ignimbrite eruption at 39 ka. *J. Volcanol. Geotherm. Res.* 327, 361–374. <https://doi.org/10.1016/j.jvolgeores.2016.09.001>.
- Tomlinson, E.L., Albert, P.G., Wulf, S., Brown, R.J., Smith, V.C., Keller, J., Orsi, G., Bourne, A.J., Menzies, M.A., 2014. Age and geochemistry of tephra layers from Ischia, Italy: constraints from 46 proximal-distal correlations with Lago Grande di Monticchio. *J. Volcanol. Geotherm. Res.* 287, 22–39. <https://doi.org/10.1016/j.jvolgeores.2014.09.006>.
- Tomlinson, E.L., Smith, V.C., Albert, P.G., Aydar, E., Civetta, L., Cioni, R., Çubukçu, E., Gertisser, R., Isaia, R., Menzies, M.A., Orsi, G., Rosi, M., Zanchetta, G., 2015. The major and trace element glass compositions of the productive Mediterranean volcanic sources: tools for correlating distal tephra layers in and around Europe. *Quat. Sci. Rev.* 118, 48–66. <https://doi.org/10.1016/j.quascirev.2014.10.028>.
- Torrente, M.M., Milia, A., Bellucci, F., Rolandi, G., 2010. Extensional tectonics in the Campanian Volcanic Zone (eastern Tyrrhenian Sea, Italy): new insights into the relationship between faulting and ignimbrite eruptions. *Ital. J. Geosci.* 129 (2), 297–315. <https://doi.org/10.3301/ijg.2010.07>.
- Tramelli, A., Giudicepietro, F., Ricciolino, P., Chiodini, G., 2022. The seismicity of Campi Flegrei in the context of an evolving long term unrest. *Sci. Rep.* 12 (1), 1–12. <https://doi.org/10.1038/s41598-022-06928-8>.
- Vineberg, S.O., Isaia, R., Albert, P.G., Brown, R.J., Smith, V.C., 2023. Insights into the explosive eruption history of the Campanian volcanoes prior to the Campanian Ignimbrite eruption. *J. Volcanol. Geotherm. Res.* 443, 107915. <https://doi.org/10.1016/j.jvolgeores.2023.107915>.
- de Vita, S., Orsi, G., Civetta, L., Carandente, A., D’Antonio, M., Deino, A., di Cesare, T., Di Vito, M.A., Fisher, R.V., Isaia, R., Marotta, E., Necco, A., Ort, M., Pappalardo, L., Piochi, M., Southon, J., 1999. The Agnano–Monte Spina eruption (4100 years BP) in the restless Campi Flegrei caldera (Italy). *J. Volcanol. Geotherm. Res.* 91 (2–4), 269–301. [https://doi.org/10.1016/s0377-0273\(99\)00039-6](https://doi.org/10.1016/s0377-0273(99)00039-6).
- de Vita, S., Sansivero, F., Orsi, G., Marotta, E., Piochi, M., 2010. Volcanological and structural evolution of the Ischia resurgent caldera (Italy) over the past 10 ky. *Geol. Soc. Am. Spec. Pap.* 464, 193–239. [https://doi.org/10.1130/2010.2464\(10\)](https://doi.org/10.1130/2010.2464(10)).
- Vitale, S., Ciarcia, S., 2018. Tectono-stratigraphic setting of the Campania region (southern Italy). *J. Maps* 14 (2), 9–21. <https://doi.org/10.1080/17445647.2018.1424655>.
- Vitale, S., Isaia, R., 2014. Fractures and faults in volcanic rocks (Campi Flegrei, southern Italy): Insight into volcano-tectonic processes. *Int. J. Earth Sci.* 103 (3), 801–819. <https://doi.org/10.1007/s00531-013-0979-0>.
- Wohletz, K., Orsi, G., De Vita, S., 1995. Eruptive mechanisms of the Neapolitan Yellow Tuff interpreted from stratigraphy, chemical, and granulometric data. *J. Volcanol. Geotherm. Res.* 67 (4), 263–290. [https://doi.org/10.1016/0377-0273\(95\)00002-c](https://doi.org/10.1016/0377-0273(95)00002-c).
- Wulf, S., Brauer, A., Mingram, J., Zolitschka, B., Negendank, J.F., 2006. Distal tephra in the sediments of Monticchio maar lakes. *La geologia del monte Vulture. Consigl. Nazion. Ricerche* 105–122.
- Wulf, S., Keller, J., Paterne, M., Mingram, J., Lauterbach, S., Opitz, S., Sottili, G., Giaccio, B., Albert, P.G., Satow, C., Tomlinson, E.L., Viccaro, M., Brauer, A., 2012. The 100–133 ka record of Italian explosive volcanism and revised tephrochronology of Lago Grande di Monticchio. *Quat. Sci. Rev.* 58, 104–123. <https://doi.org/10.1016/j.quascirev.2012.10.020>.
- Zanchetta, G., Sulpizio, R., Giaccio, B., Siani, G., Paterne, M., Wulf, S., D’Orazio, M., 2008. The Y-3 tephra: a last Glacial stratigraphic marker for the Central Mediterranean basin. *J. Volcanol. Geotherm. Res.* 177 (1), 145–154. <https://doi.org/10.1016/j.jvolgeores.2007.08.017>.
- Zernack, A.V., Cronin, S.J., Neall, V.E., Procter, J.N., 2011. A medial to distal volcanoclastic record of an andesite stratovolcano: detailed stratigraphy of the ring-plain succession of south-West Taranaki, New Zealand. *Int. J. Earth Sci.* 100 (8), 1937–1966. <https://doi.org/10.1007/s00531-010-0610-6>.